THE JOURNAL OF BIOLOGICAL CHEMISTRY VOL. 287, NO. 45, pp. 37673–37690, November 2, 2012

SPAK Isoforms and OSR1 Regulate Sodium-Chloride Co-transporters in a Nephron-specific Manner*

Received for publication, July 19, 2012, and in revised form, August 28, 2012 Published, JBC Papers in Press, September 12, 2012, DOI 10.1074/jbc.M112.402800

P. Richard Grimm[‡], Tarvinder K. Taneja[‡], Jie Liu[‡], Richard Coleman[‡], Yang-Yi Chen[‡], Eric Delpire[§], James B. Wade[‡], and Paul A. Welling[‡1]

From the [‡]Department of Physiology, University of Maryland School of Medicine, Baltimore, Maryland 21201 and the [§]Department of Anesthesiology, Vanderbilt University School of Medicine, Nashville, Tennessee 37232

Background: Full-length SPAK is thought to be necessary and sufficient to activate NCC in the distal convoluted tubule (DCT).
Results: SPAK knock-out disrupts a signaling network, involving OSR1, in the DCT but not the TAL, preventing NCC activation.
Conclusion: SPAK and OSR1 function interdependently in the DCT to positively regulate NCC.
Significance: This study provides insights into the mechanisms whereby SPAK/OSR1 regulates renal salt transport.

STE20/SPS-1-related proline-alanine-rich protein kinase (SPAK) and oxidative stress-related kinase (OSR1) activate the potassium-dependent sodium-chloride co-transporter, NKCC2, and thiazide-sensitive sodium-chloride cotransporter, NCC, *in vitro*, and both co-localize with a kinase regulatory molecule, Cab39/MO25α, at the apical membrane of the thick ascending limb (TAL) and distal convoluted tubule (DCT). Yet genetic ablation of SPAK in mice causes a selective loss of NCC function, whereas NKCC2 becomes hyperphosphorylated. Here, we explore the underlying mechanisms in wild-type and SPAK-null mice. Unlike in the DCT, OSR1 remains at the TAL apical membrane of KO mice where it is accompanied by an increase in the active, phosphorylated form of AMP-activated kinase. We found an alterative SPAK isoform (putative SPAK2 form), which modestly inhibits co-transporter activity *in vitro*, is more abundant in the medulla than the cortex. Thus, enhanced NKCC2 phosphorylation in the SPAK knock-out may be explained by removal of inhibitory SPAK2, sustained activity of OSR1, and activation of other kinases. By contrast, the OSR1/SPAK/M025α signaling apparatus is disrupted in the DCT. OSR1 becomes largely inactive and displaced from M025α and NCC at the apical membrane, and redistributes to dense punctate structures, containing WNK1, within the cytoplasm. These changes are paralleled by a decrease in NCC phosphorylation and a decrease in the mass of the distal convoluted tubule, exclusive to DCT1. As a result of the dependent nature of OSR1 on SPAK in the DCT, NCC is unable to be activated. Consequently, SPAK$^{-/-}$ mice are highly sensitive to dietary salt restriction, displaying prolonged negative sodium balance and hypotension.

Two closely related kinases, Ste20-related proline-alanine-rich kinase (SPAK)[2] and the oxidative stress-responsive kinase 1 (OSR1), are well appreciated to phosphoregulate cation-dependent chloride transporters. Both have been implicated in controlling the activity of NKCC2 and NCC, the co-transporters responsible for salt reabsorption in the thick ascending limb and distal convoluted tubule (1–7). As the two individual members of the germinal center kinase VI subfamily of STE20 kinases (8), SPAK and OSR1 exhibit a high degree of structural homology, and share similar common domain architectures. Both contain an N-terminal kinase domain, a kinase regulatory domain, and a C-terminal substrate-binding domain (9). Based on studies in heterologous expression systems, SPAK and OSR1 also appear to exhibit identical functional properties. Both kinases specifically bind to a (S/G/V)RF*X*(V/I)*XX*(V/I/T/S) motif found in NKCC1, NKCC2, and NCC (5, 10–12), and upon interaction, both kinases phosphorylate a conserved cluster of threonine and serine residues located within the N terminus of the transporters. Because phosphorylation of these residues is necessary for cotransporter activation (5, 6), it has been suspected that OSR1 and/or SPAK are required to maintain NKCC2 and NCC activity *in vivo*. Based on the common structural and catalytic properties of SPAK and OSR1, and reports that SPAK and OSR1 may be co-expressed in the thick ascending limb (TAL) and the distal convoluted tubule (DCT) (3, 7), it was presumed that the kinases perform functionally redundant activities, phosphorylating NKCC2 and NCC to maintain sodium reabsorption in the thick ascending limb and distal convoluted tubule.

Recent studies with genetically engineered mouse models of kinase loss-of-function reveal the physiologic roles of SPAK/OSR1 signaling in the kidney are unexpectedly much more complex (3, 4, 7). Yang and collaborators (7) reported that SPAK knock-out mice exhibit hypotension, hyperaldosteronism, and a salt-wasting disorder that is surprisingly restricted to the DCT, recapitulating Gitelman syndrome, a human disease caused by loss-of-function mutations in NCC (13). Consistent with the unanticipated highly focused phenotype, phosphorylation of NCC, but not NKCC2, is attenuated in these SPAK knock-out mice. Remarkably, SPAK gene ablation actually leads to an increase in NKCC2 phosphorylation (2), a phenotype that seems to be absent in the catalytically inactive SPAK knock-in mouse (4). Examining a different SPAK null strain,

* This work was supported, in whole or in part, by National Institutes of Health Grants 1RC1DK086817 (to P. A. W.), DK32839 (to J. B. W.), GM074771 (to E. D.), and 5T32HL072751 (to P. R. G.).
[1] To whom correspondence should be addressed. Tel.: 410-706-3851; Fax: 410-706-8341; E-mail: pwelling@umaryland.edu.
[2] The abbreviations used are: SPAK, Ste20-related proline-alanine-rich kinase; ORS1, oxidative stress-responsive kinase 1; TAL, thick ascending limb; DCT, distal convoluted tubule; AMPK, AMP-activated protein kinase.

which has been reported to be surprisingly normotensive and have normal levels of aldosterone, McCormick *et al.* (3) suggested that removal of a TAL-specific inhibitory SPAK isoform, KS-SPAK, in the $SPAK^{-/-}$ mice would allow OSR1 to hyperphosphorylate NKCC2. Nevertheless, it is not clear what leads to the differences in the phenotype of the two SPAK null mice strains, and many key aspects of this intriguing SPAK isoform hypothesis remain untested. Most importantly, our understanding of the mechanisms underlying the apparent nephron segment-specific functions of SPAK and OSR1 are incomplete. Given the similar expression of OSR1 in the DCT as well as in the TAL, it remains especially mysterious why basal sodium transport in the DCT is so profoundly dependent on SPAK.

The requirements of SPAK and OSR1 in the physiological stimulation of NCC also remain unclear. Phosphorylation and abundance of NCC at the apical membrane are up-regulated in states of high angiotensin II and aldosterone when dietary salt is restricted and intravascular volume is low. This important regulatory response is coincident with phosphorylation of SPAK and OSR1 at their key activation sites (SPAK, Thr-243, Ser-383; OSR1, Thr-185, Ser-325) (1, 5, 14, 15), but a causal link between physiological stimulation of NCC and SPAK/OSR1 activation has not been firmly established. Results from *in vitro* studies suggest that the effects of aldosterone/angiotensin II signaling on NCC phosphorylation are communicated through the *w*ith *no* lysine-*K* kinases (WNK1/4), which phosphorylate and activate SPAK and OSR1. Consistent with this idea, aberrant stimulation of NCC phosphorylation in mouse models of pseudohypoaldosteronism type II (PHAII), a familial disease of hypertension and hyperkalemia caused by mutations in WNK1 and WNK4 (16–20), is pathologically driven by heightened activation of SPAK and OSR1 (4, 17). Recent studies with WNK4 KO mice indicate that physiologic activation of SPAK, OSR1, and NCC by a low sodium diet are all dependent on WNK4 (21). However, the requirement for regulatory co-factors, such as the calcium-binding protein 39 (Cab39, also called mouse protein-25, MO25), which activates SPAK/OSR1 *in vitro* by binding to and stabilizing the active conformation (22, 23) is presently unknown. Most importantly, it still remains unclear whether SPAK, OSR1, or both kinases are required for physiological stimulation of NCC. The present study is designed to address these key and timely questions about disparate SPAK/OSR1 signaling in the TAL and DCT, particularly to elucidate why basal and regulated activity of NCC is so dependent on SPAK.

EXPERIMENTAL PROCEDURES

Animals—The University of Maryland School of Medicine Institutional Animal Care and Use Committee approved all procedures. The generation of SPAK knock-out (KO, $SPAK^{-/-}$) mice has been described in detail previously (11, 24). Briefly, the SPAK gene (*Stk39*) was disrupted by duplicating exon 6 and inserting tyrosinase (*Tyr*), neomycin resistance (*neo*), and 50 hypoxanthine phosphoribosyltransferase (*hprt*) genes between the two exons. These mice differ from the $SPAK^{-/-}$ mice generated by Yang *et al.* (7), which were produced by disrupting the SPAK gene through deletion of exons 9 and 10. Six mice (4 females and 2 males), heterozygous for SPAK deletion (Het, $SPAK^{+/-}$), were transferred from Vanderbilt University to the University of Maryland School of Medicine and backcrossed further in C57BL6. Heterozygous male and female mice were bred to expand the colony and generate mice for experimentation. The heterozygous crossing generated wild-type (WT, $SPAK^{+/+}$) and $SPAK^{-/-}$ pups in the expected Mendelian ratio of 25% $SPAK^{+/+}$, 25% $SPAK^{-/-}$, 50% $SPAK^{+/-}$. Male pups were screened by PCR genotyping of tail DNA to distinguish WT from Het and KO. As PCR based strategy cannot distinguish Het and KO animals, the final determination of genotype was assessed by Western blotting of either kidney lysate following animal sacrifice or protein isolated from primary cultures of tail fibroblasts. Experimental cohorts were arranged such that WT and KO littermates were paired and equally represented. The animals were housed in the animal facility within the University of Maryland School of Medicine in groups of two to five per cage. The colony room was maintained on a 12:12 h light/dark cycle; with lights on at 6 a.m. Food and water were available *ad libitum*.

While this manuscript was in preparation, McCormick *et al.* (3) published the results of studies on the same genotype of SPAK null mice. It should be pointed out that there are a few significant differences. The SPAK null mice studied here were bred in C57BL6 for greater than 10 generations, and are therefore essentially pure C57BL6, and slightly different from the chimeric mice (generation F6, 98.5% C57BL6) examined by McCormick *et al.* (3). More importantly, we studied younger mice (8–10 weeks) than McCormick *et al.* (3) (3–5 months old).

Dietary Manipulation—After determining genotype (~6 weeks old), the animals were given a control diet (1% potassium, 0.32% sodium, 0.9% chloride; TD.88238). At ~8 weeks of age the animals were assigned to a dietary regimen that consisted of either: 1) the control diet or 2) sodium-deficient diet matched for equal caloric intake to the control diet (1% potassium, 0.01% sodium, 0.45% chlorine; TD.10431). The animals were acclimated to these diets for 10 days and then studied. All diets were purchased from Harlan Teklad and designed with assistance of a Teklad certified dietician.

Metabolic Cage Studies—Animals were placed in a diuresis metabolic cage for mice (Nalgene) and allowed to adapt for 3 days. Following this period, food and water consumption was determined and urine samples were collected for an additional 3 days. Urine samples were collected several times a day to prevent contamination from food, water, and fecal matter. Additionally, urine samples flowed to a collection tube containing mineral oil to prevent evaporation.

Blood Pressure Measurements—Conscious blood pressure measurements were made using a DSI (Data Sciences International) telemetry based system. PA-C10 telemeters were surgically implanted following the manufacturer's instruction. Following the surgery, the animals were allowed to recover for 4 days before beginning measurements. Dataquest ART 4.2 software was used to create a sampling program that measured the blood pressure of each animal for 20 s every 10 min.

Sample Collection, Preparation, and Analysis—Animals were anesthetized by intraperitoneal injection with ketamine/xylazine (100 mg/kg of ketamine, 10 mg/kg of xylazine). Once an animal was unconscious, the left renal artery was completely

ligated and the left kidney was removed, dissected into cortex and medulla samples, and flash frozen in liquid nitrogen. Blood samples were collected from the carotid artery and immediately spun-down to separate the blood cells from the plasma. The plasma was isolated and frozen for later analysis of electrolytes, aldosterone, and creatinine. Plasma and urine samples were sent to IDEXX Preclinical Research Laboratories for electrolyte analysis. Plasma and urine creatinine levels were measured in our lab using the QuantiChrom Creatinine Assay Kit (BioAssay Systems) following the manufacturers protocol. Plasma aldosterone levels were assayed using the Aldosterone EIA Kit manufactured by Cayman Chemical.

Antibodies—The following antibodies were used for Western blotting and immunolocalization studies (in all cases sequence numbers refer to that in mouse): rabbit anti-NCC, amino acids 104–122; chicken anti-pNCC T58, amino acids 54–66; rabbit anti-NKCC2, kindly provided by M. Knepper (25); rabbit anti-pNKCC2, R5, kindly provided by B. Forbush (26); rabbit anti-SPAK (12); rabbit anti-OSR1 (27); rabbit anti-MO25α (Cell Signaling Technology); and rabbit anti-phospho-AMPKα (Thr-172) (Cell Signaling Technology). The following antibodies raised in sheep were obtained from the Division of Signal Transduction Therapy at the University of Dundee, Dundee, UK: total SPAK, amino acids 196–210 (S150C); total OSR1, amino acids 333–352 (S149C); pSPAK/OSR1, Ser-383/Ser-325 (S670B); pSPAK/OSR1, Thr-243/Thr-185 (S204C). Studies using anti-phosphoantibodies used an excess of nonphosphopeptide to block possible nonspecific labeling in both immunoblotting and localization studies. Immunolocalization studies used not only the above antibodies but guinea pig anti-NCC and chicken anti-NKCC2 (28), mouse anti-parvalbumin (Millipore), rabbit anti-parvalbumin (Swant), and rabbit anti-calbindin-D (Cell Signaling Technology).

Immunolocalization—Anesthetized mice were fixed by perfusion with 2% paraformaldehyde in PBS via the left ventricle for 5 min at room temperature. The kidneys were then removed and fixed an additional 24 h at 4 °C in the same fixative, rinsed in PBS, and embedded in paraffin. Cross-sections 3-μm thick, cut at the level of the papilla, were picked up on chrome-alum gelatin-coated glass coverslips and dried on a warming plate. The sections were then deparaffinized in two xylene baths and two absolute ethanol baths, 5 min each, and rehydrated in a graded ethanol series to distilled water.

For epitope retrieval, the coverslips were placed in a pH 8 aqueous solution of Tris (1 mM), EDTA (0.5 mM), and SDS (0.02%). The retrieval solution was heated to boiling in a microwave oven, transferred to a conventional boiling water bath for 15 min, and then allowed to cool to room temperature before the sections were thoroughly washed in distilled water to remove the SDS.

Sections were preincubated for 30 min with Image-iT blocking solution (Invitrogen), rinsed in PBS, and then preincubated an additional 30 min in a solution of 2% BSA, 0.2% fish gelatin, 5% normal donkey serum, and 0.2% sodium azide in PBS. Tissues were thoroughly rinsed with Tris-buffered saline (TBS) to remove PBS. Incubations with specific antibodies (as described above), diluted in TBS containing 1% BSA, 0.2% fish gelatin, 0.1% Tween 20, 10 mM $CaCl_2$, and 0.2% sodium azide, took place overnight in a humid chamber at 4 °C. After thorough washing in high salt wash (incubation medium plus added sodium chloride at 0.5 M), the anti-parvalbumin was detected with Alexa Fluor 488-conjugated donkey anti-mouse IgG (Jackson Laboratories); anti-sodium chloride cotransporter was detected with Alexa Fluor 568-conjugated donkey anti-guinea pig IgG (Jackson Laboratories); and anti-calbindin-D was detected with DyLight 649-conjugated donkey anti-rabbit IgG (BioLegend). Unconjugated secondary antibodies from Jackson Laboratories were coupled to the respective fluorophores using kits from Invitrogen.

Image Analysis—Quantitative analysis of confocal images (fluorescence intensity and co-localization) was performed using Improvision Volocity 5 by a trained investigator who was blind as to identity of the sample groups.

Morphometric Analysis of DCT in Kidney Sections—Histological sections were cut perpendicular to the surface and passed through the center of each kidney allowing quantification of DCT length and area throughout the entire cortex. Complete cortical regions of immunolocalized sections of kidneys from test animals were photographed with a Zeiss LSM 410 confocal microscope using a $\times$10 objective lens and filters appropriate for the fluorophores used. Using the three fluorophore colors, the two regions of the DCT could be identified for quantification: red (NCC) for the total DCT, green (parvalbumin) for the DCT1, and blue (calbindin) for the DCT2. Every NCC-containing tubule in each tissue section was classified using this system.

As measured by an examiner who was blind to the identity of the two groups (WT *versus* SPAK null), total DCT1 and DCT2 lengths were determined with a curvilinear test system developed by Merz (29). This system of interconnected semicircles is independent of the grid orientation relative to the boundary being measured. For the test grid, $B = I_i d$, where B is the linear boundary length being measured, I_i is the number of intersections between the curvilinear test grid and the boundary, and d is the diameter of the grid semicircles (21 μm). The boundary in this case was one outer edge of the tubule being measured, but limited by the axial extent of the NCC-labeled apical membrane.

The test grid also contained a small dot at the midpoint of each semicircle. The dots were used in point counting to measure the total tubular area of DCT1 and DCT2. The area fraction of tubules of each type was calculated by dividing the number of dots falling on each tubule type by the total number of dots falling on the cortex. The dots on the grid were 21 μm apart, and thus each dot represented 421 μm^2 of area. Using this conversion, the area fraction could be expressed as $\mu m^2/mm^2$.

Sample Preparation for Western Blotting—Mouse kidney tissue (cortex/medulla) was sonicated in HEENG buffer (20 mM Hepes (pH 7.6), 125 mM NaCl, 1 mM EDTA, 1 mM EGTA, 10% glycerol) containing 1% Triton and 0.5% SDS with protein and phosphatase inhibitor. Samples were sonicated 3 times at 10-s pulses. The samples were rotated at 4 °C for 1 h at low speed (7,500 rpm) and then spun down at high speed (15,000 rpm) for 10 min to pellet insoluble material. The supernatant was collected and quantified for protein yield using a bicinchoninic

acid protein assay reagent kit (Pierce). Equal amounts of kidney protein were suspended in Laemmli buffer (room temperature for 45 min) and resolved on 8 (NKCC2 and NCC) or 10% (SPAK and OSR1) SDS-PAGE gels, and transferred to Amersham Biosciences Hybond-ECL membranes and blocked in Tris-buffered saline with 0.1% Tween 20 (TBS-T) containing 5% nonfat dry milk for 1 h at room temperature. Membranes were then incubated in 5% nonfat dry milk containing primary antibody (4 °C, overnight), washed in TBS-T, incubated in 5% nonfat dry milk containing HRP-conjugated secondary antibody, and then washed for 10 min (3 times) in TBS-T. Bound antibodies were then revealed using enhanced chemiluminescence reagent (Pierce) and fluorography. The integrated densities of bands (corresponding to total or phosphorylated NCC, NKCC2, SPAK, OSR1, and β-actin) were measured using Image J software (NIH). Unless otherwise stated, each protein signal was divided by its own β-actin signal to yield an actin-normalized signal. These data are presented and analyzed as the relative abundance, denoting the actin-normalized test signal relative to the average of the wild-type normalized signal.

RNA Isolation and Real-time PCR—Total RNA was isolated from renal tissue using TRIzol (Invitrogen) and then reverse-transcribed with Superscript III (Invitrogen) and oligo(dT) primers, each per the manufacturer's protocol. Real-time PCR experiments were performed using a LightCycler 480 system and LightCycler 480 SYBR Green Master Mix (Roche Applied Science). Primer sets for β-actin (reference transcript), parvalbumin, calbindin, NCC, and NKCC2 were designed using MacVector. The efficiency value (*E*-value) of each primer set was calculated using LightCycler 480 software based on the threshold cycle number (C_T) of 3-sets of serially diluted control samples each run in triplicate. An efficiency of 100% represents a doubling over the enter range of diluted samples and is assigned a value of 2, whereas a primer set that amplified with an efficiency of 98% is assigned a value of 1.98. Each primer set had an *E*-value greater than 1.92. Using the efficiency value of a give target, the relative transcript abundance is calculated by raising the *E*-value by a power equal to the change in threshold cycle number (ΔC_T) and dividing the product by the corresponding efficiency and ΔC_T value of the reference transcript. The sequence of the primers is as follows: β-actin (*Actb*) (Fwd), GGCATTGTTACCAACTGGGACG and (Rev) CTCTTTGATGTCACGCACGATTTC; parvalbumin (*Pvalb*) (Fwd), TTCCAGATGGTGGGCCTGAAG and (Rev) AGACAAGTCTCTGGCATCTGA; calbindin (*Calb1*) (Fwd), CTAGCAGAGTACACAGACCTC and (Rev) GTATCCGTTGCCATCCTGATC; NCC (*Slc12a3*) (Fwd), GGGTTTGTGTCATGAGGATG and (Rev) AGATGGTGGTGGCCTGCTC; and NKCC2 (*Slc12a1*) (Fwd), CCTTTGACTTTGAGATTGGCGTG and (Rev) GGGCTGGCTTGGTAATGTTCAG.

Oocyte Expression Studies—SPAK2 was created using full-length mouse SPAK cDNA (*Stk39*) and PCR amplification of a short fragment. The forward primer (GAATTCAGCATCATGGATGAACTCCTGAAAG) included an EcoRI site at the 5′ end and sequences starting at Met-115. The reverse primer (GATATCCAACATGGAACCTCCACTTAG) included a unique internal EcoRV site. After amplification, the fragment was ligated into pGEM-T Easy (Promega) and sequenced. Finally, the EcoRI-EcoRV 5′ fragment from full-length SPAK was substituted with the EcoRI-EcoRV PCR fragment. The constitutively active SPAK (T243E and S383D) was previously described (30). All clones are inserted into pBF, an oocyte expression vector.

Stage V or VI oocytes were isolated from *Xenopus laevis* frogs as described by Delpire and Gagnon (30). All husbandry and surgical procedures were approved by the Vanderbilt University Animal Care and Use Committee, and were in compliance with United States Public Health Service Policy on humane care and use of laboratory animals. The day after isolation, oocytes were injected with 50 nl of water containing 15 ng of mouse NKCC1 cRNA. The third day, oocytes were injected with 50 nl of water containing 10 ng of each kinase cRNA (11). K^+ uptakes were measured on day 5 by using 5 mCi/ml of ^{86}Rb, as tracer. Detailed flux methodology can be found in earlier publications (11, 30). Previous studies have demonstrated that >90% of the uptake is mediated by NKCC1 (30). Fluxes were expressed in nanomoles of K^+ per oocyte per h. Data were analyzed using Instat's analysis of variance test followed by Tukey-Kramer Multiple Comparisons Test (GraphPad, La Jolla, CA).

Statistical Analysis—Data are presented as mean ± S.E. For mouse studies, each "*n*" represents a different animal. Statistical analysis was performed using GraphPad PRISM version 5. Statistical significance was determined by *t* test when comparing two groups and by one-way randomized analysis of variance followed by Bonferroni's post hoc test when comparing multiple groups or Dunnett's post hoc test when multiple test groups were compared with the control. $p < 0.05$ was considered significant.

RESULTS

Decompensated Gitelman Phenotype in Young SPAK Null Mice

To begin to understand why salt reabsorption in the distal convoluted tubule might be so profoundly dependent on SPAK, compared with the thick ascending limb, we first sought to settle a puzzling phenotype issue between different SPAK null mice (7, 11, 24). One strain of mice, generated and studied by Yang *et al.* (7), exhibit frank hypotension, volume contraction, and hyperaldosteronism, whereas the other strain, generated by Delpire and Gagnon (11, 24) and as studied by McCormick *et al.* (3) do not exhibit hypotension or hypoaldosteronism. To shed light on these disparities, we considered the possibility that the mice studied by McCormick *et al.* (3) might be more compensated than the mice studied by Yang. Accordingly, we carefully assessed the renal and blood pressure phenotype of the Delpire SPAK null mice (24), but we purposely evaluated younger mice (8–10 weeks) than examined by McCormick *et al.* (3) to limit the influence of potential compensatory factors.

As summarized in Fig. 1 and Table 1, we found these SPAK null mice exhibit a more decompensated phenotype than previously reported (3). Unlike the mice studied by McCormick *et al.* (3), which are normotensive, our telemetric measurements of blood pressure revealed the younger $SPAK^{-/-}$ mice are hypotensive, particularly during the active, awake period (Fig. 1). As evidenced by the elevated plasma aldosterone and BUN

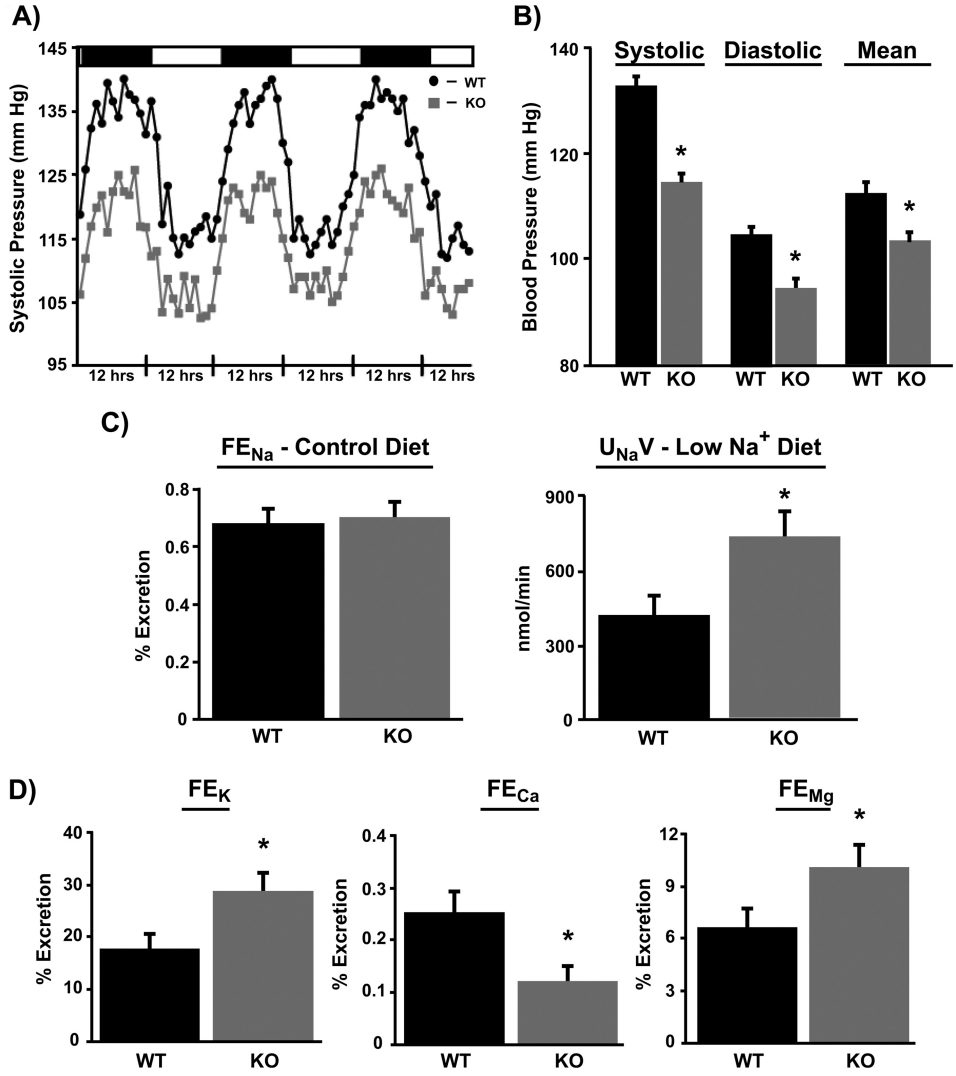

FIGURE 1. **Hypotension and altered urinary excretion of sodium and divalent cations in SPAK$^{-/-}$ mice, recapitulating decompensated Gitelman syndrome.** *A*, 72-h telemetric analysis of systolic blood pressure established that SPAK$^{-/-}$ mice maintain the typical diurnal variation (*black bar*, night; *white bar*, day) in blood pressure (*A*; $n = 4$), but as summarized in *B* plots of systolic, diastolic, and mean blood pressure (measured at night), SPAK$^{-/-}$ mice are hypotensive during their active period (*B*; $n = 4$, *, $p < 0.05$). Renal function studies: *C*, fractional excretion of sodium (FE$_{Na}$) of WT and SPAK$^{-/-}$ mice are equal when fed the control diet but as measured by the rate of urinary sodium excretion (U$_{Na}$V, 6 h after switched to low sodium), the SPAK$^{-/-}$ mice display significant sodium wasting when fed a sodium-deficient diet (*C*; $n = 8$). SPAK$^{-/-}$ have increased fractional excretion of potassium and magnesium, as well as a decreased fractional excretion of calcium (*D*; $n = 8$). *, $p < 0.05$.

(Table 1), the hypotension occurs concomitantly with a more profound intravascular volume contraction than reported in the study by McCormick *et al.* (3). Although differences in age may explain these phenotypic differences, we cannot rule out that other factors, such as subtle differences in genetic background (see "Experimental Procedures") and diet, are also contributory. In any regard, our model offers a means to examine direct effects of SPAK ablation before compensatory processes confound interpretation.

Renal function measurements provide insight into the basis of the phenotype (Fig. 1). SPAK null mice have a normal GFR and maintain salt balance on a normal sodium diet, but exhibit a propensity to waste sodium when challenged with a low sodium diet. They also display an increased fractional excretion of potassium (FE$_K$) and tend to be slightly hypokalemic although plasma potassium values are not significantly different from WT. Alterations in urinary excretion of divalent cations, namely an increased fractional excretion of magnesium and decreased fractional excretion of calcium, are identical to those observed in NCC knock-out mice (31). In fact, the entire phenotype recapitulates Gitelman syndrome as observed by Yang *et al.* (7) in a different SPAK null strain, consistent with a specific defect in NCC-dependent sodium reabsorption in the DCT.

Evaluation of NCC and NKCC2 protein abundance and phosphorylation by semiquantitative Western blotting provides insight into the basis of the Gitelman phenotype (Fig. 2). As shown in the representative blots (Fig. 2*A*), and quantitative summary (Fig. 2*B*), the total and phosphorylated NCC is significantly attenuated in SPAK$^{-/-}$ mice compared with WT mice. In contrast to NCC, abundance of the NKCC2 protein is not altered and the major phosphorylated form of NKCC2 is increased in the SPAK$^{-/-}$ mice. These observations verify that SPAK acts as a critical positive regulator of NCC, but not of NKCC2.

TABLE 1
Physiological parameters of WT and SPAK$^{-/-}$ mice

Parameter	Genotype	
	WT ($n = 8$)	SPAK$^{-/-}$ ($n = 8$)
Weight (g)	22.7 ± 1.9	21.7 ± 0.9
Food intake (g/day)	2.6 ± 0.3	2.8 ± 0.4
Water intake (ml/day)	4.1 ± 0.5	4.2 ± 0.4
Plasma		
Sodium (mM)	141.5 ± 1.5	139 ± 1.8
Potassium (mM)	3.9 ± 0.3	3.3 ± 0.3
Chlorine (mM)	113.0 ± 2.3	108.7 ± 2.4
Calcium (mM)	8.4 ± 0.9	8.2 ± 0.5
Magnesium (mM)	2.9 ± 0.3	2.2 ± 0.4
BUN (mg/dl)	23.0 ± 2.3	28.6 ± 2.8[a]
Creatinine (mg/dl)	0.37 ± 0.09	0.35 ± 0.11
Aldosterone (pg/ml)	430 ± 70	810 ± 110[a]
Urine		
Volume (ml/day)	3.3 ± 0.3	3.5 ± 0.3
Sodium (μmol/day)	220.3.2 ± 30.7	236.9 ± 39.0
Potassium (μmol/day)	452.8 ± 36.3	532.8 ± 46.9
Chlorine (μmol/day)	161.5 ± 23.1	168.8 ± 27.3
Magnesium (μmol/day)	118.0 ± 10.0	119.0 ± 9.0
Calcium (μmol/day)	10.8 ± 0.9	6.5 ± 0.5[a]
Creatinine (mg/dl)	50.1 ± 9.3	47.4 ± 12.0
Apparent GFR (μl/min)	313.5 ± 23.0	323.5 ± 29.4

[a] $p < 0.05$, SPAK$^{-/-}$ relative to littermate WT mice.

SPAK Is Required to Maintain Basal Phosphorylation of NCC and DCT1 Cell Mass

Heterologous expression studies previously established that SPAK (and OSR1)-mediated phosphorylation of NCC controls the activity of the transporter, rather than its abundance (5, 10). Thus, the impressive reduction of NCC protein in SPAK null mice indicates that SPAK has unappreciated, more complex regulatory functions *in vivo*. To elucidate the underlying mechanisms, we examined how SPAK gene ablation affects DCT structure, NCC abundance, and phosphorylation at organ and cell levels.

Visualization of the kidney cortex by immunofluorescence microscopy at low power reveals the reduction in NCC protein abundance is paralleled by a major structural disruption of the DCT (Fig. 3*A*) within the parvalbumin-positive DCT1 segment. As quantified by morphometric analysis (Fig. 3*B*), we found the DCT1 segment is significantly smaller in SPAK$^{-/-}$ mice compared with WT. Semiquantitative RT-PCR revealed for the first time a corresponding decrease in transcript abundance of NCC and parvalbumin, whereas the abundance of calbindin (DCT2 marker) and NKCC2 (TAL marker) transcripts remained unaffected (Fig. 3*D*). By examining several DCT markers, rather than NCC alone as done previously (3, 7), our observations provide unambiguous evidence that the mass of the DCT, specifically the DCT1, is reduced in SPAK null mice. Collectively, these studies identify SPAK as part of a signaling pathway that maintains the integrity of distal convoluted tubule, and thereby controls NCC abundance, and NCC-dependent sodium reabsorption.

Observations at the cellular level provide insight into how SPAK may control DCT mass (Fig. 4). Within remnant DCT tubules of SPAK$^{-/-}$ mice, NCC remains localized to the apical membrane. As assessed by confocal microscopy (Fig. 4*A*) and quantitative image analysis (Fig. 4*B*), phosphorylation of NCC per cell is strikingly attenuated in the SPAK null compared with the modest reduction in total abundance of NCC per remnant DCT cell (Fig. 4*A*). We interpret these observations to indicate that SPAK is primarily required to maintain the activity of NCC within individual DCT, rather than control apical localization. It may have a role in controlling NCC abundance in the cell, but this is minor compared with its role in activating transporters by phosphorylation. Because maintenance of the distal convoluted tubule is well appreciated to depend on NCC-mediated sodium transport (32, 33), we propose that the dystrophic DCT response in SPAK$^{-/-}$ mice is largely initiated by impaired phosphoregulation of NCC activity. By contrast, SPAK is not required to maintain NKCC2 activity in the thick ascending limb. As evidenced by the higher levels of phosphorylated NKCC2 at the TAL apical membrane in the SPAK$^{-/-}$ mice compared with WT mice (see Fig. 7*C, below*), SPAK knock-out actually produces a stimulatory, rather than inhibitory, response in the TAL.

Disparate SPAK-dependent Signaling Pathways in the Thick Ascending Limb and Distal Convoluted Tubule

Role of Different SPAK Forms—The contrasting responses of NCC and NKCC2 phosphorylation to SPAK gene ablation suggest the SPAK-dependent signaling pathways in the thick ascending limb and distal convoluted tubules are fundamentally different. As a first step to examine how different they might be, Western blotting of SPAK in WT and SPAK$^{-/-}$ kidneys were performed (Fig. 5*A*). For these studies, kidney cortex was dissected from the outer medulla to separate regions of kidney containing DCTs from those that have medullary thick ascending limbs (mTAL).

As shown in Fig. 5*A*, two major protein species of SPAK (~58 and 60 kDa), migrating near the predicted molecular mass of full-length SPAK (60 kDa), were detected in the kidney cortex and medulla of wild-type mice. Smaller molecular mass SPAK forms (~46 and 48 kDa) were almost always detected in the outer medulla of WT mice (90% of mice tested), usually in combination with the full-length forms. By contrast, smaller forms in the cortex were observed in only half of the samples, were not as abundant as those in medulla, and were always in combination with the full-length forms (Fig. 5*B*). Although the differences in the SPAK expression patterns between kidney cortex and medulla are more variable than previously described (3), our observations support the idea that favored expression of smaller SPAK forms in the TAL might cause the SPAK/OSR1 signaling system to behave differently than in the DCT.

It should be pointed out that the smaller fragments that we detect are larger than the predicted size (34 kDa) of the kidney-specific kinase, KS-SPAK. We considered the possibility that the smaller SPAK form might, instead, correspond to SPAK2, a short form generated by alterative initiation of translation (27) or a comparable proteolytic fragment, because SPAK2 exhibits comparable molecular mass to these forms (predicted molecular mass of SPAK2 is 49 kDa). SPAK2 was proposed to be kinase-inactive (27), but its activity has never been tested.

Accordingly, to address the function of SPAK2, we co-expressed it with the prototypic sodium-dependent chloride cotransporter, NKCC1, in *X. laevis* oocytes in the absence and presence of a constitutively active SPAK kinase (CA-SPAK), and measured co-transporter activity. By itself, SPAK2 induced a significant inhibitory effect on NKCC1 function (Fig. 5*D*),

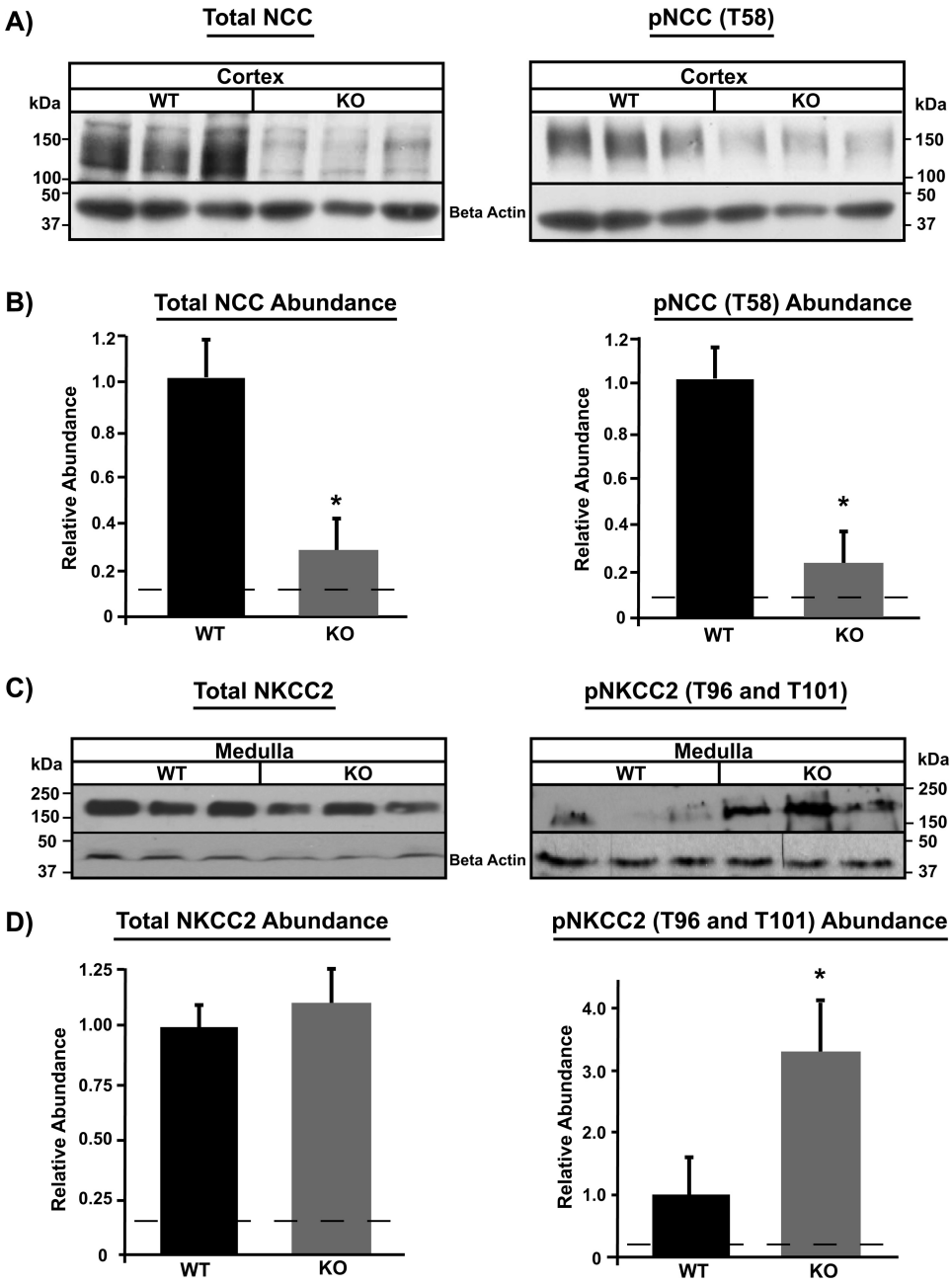

FIGURE 2. **SPAK positively regulates NCC but not NKCC2.** Representative Western blots and quantitative summary of NCC abundance (*A*) total and (*B*) phosphorylated (pNCC, Thr-58). Compared with WT, total and pNCC are significantly attenuated in SPAK$^{-/-}$ mice (*KO*). Relative abundance is the actin-normalized signal relative to the average of the wild-type actin-normalized signal. The *dashed line* represents the amount of signal attributable to background. $n = 9$, *, $p < 0.05$, KO compared WT. *C,* total NKCC2 protein abundance in SPAK$^{-/-}$ animals not statistically different from WT. *D*, the abundance of the major phosphorylated form of NKCC2 as detected with the anti-pNKCC2 (Thr-96/Thr-101) antibody is increased in the SPAK$^{-/-}$ mice, within the outer medulla (*C* and *D*). Quantitative summary represent an $n = 6$, *, $p < 0.05$, KO relative to WT.

likely by overwhelming the stimulatory effects of endogenous OSR1, which drives basal NKCC1 activity in oocytes. Surprisingly, when co-expressed with the catalytically active SPAK kinase, SPAK2 did not significantly inhibit NKCC1. Taken together, these studies indicate that SPAK2 has the capacity to inhibit NKCC1, but its ability to act as a negative regulator can be mitigated when the active, full-length SPAK form is abundant. Thus, the inhibitory activity of SPAK2 is much less potent than the large negative effects reported for the KS-SPAK form (3). To test the potential relevance of this phenomenon in the TAL, we carefully evaluated the relative abundance of the different SPAK forms in the outer medulla. As shown in Fig. 5*E*, the shorter SPAK forms are expressed in nearly equal abundance as the full-length forms under basal conditions. Furthermore, dietary salt restriction increased all SPAK forms in the medulla (Fig. 5*F*), without a significant change in the relative abundance of the long and short forms. We infer from these observations that the inhibitory activity of the shorter SPAK forms in the TAL has the potential to dampen NKCC2 but this is not likely to exceed the stimulatory activity of full-length SPAK as proposed by McCormick *et al.* (3). Thus, loss of the inhibitory SPAK2 isoform in TAL is predicted to have a modest

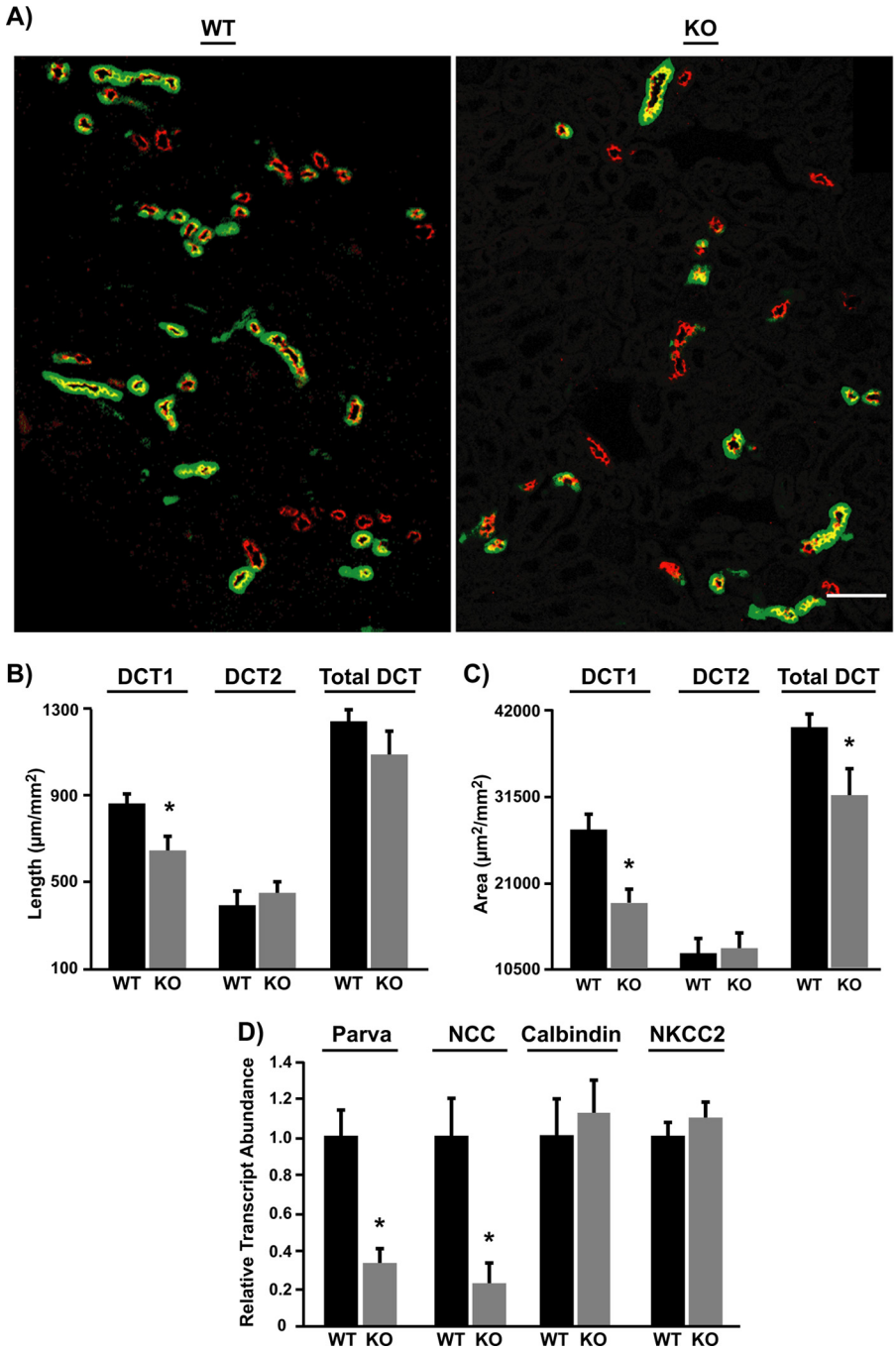

FIGURE 3. **Cellular mass of DCT1 is specifically reduced in SPAK$^{-/-}$ *mice.*** *A,* representative low magnification views of kidney cortex in WT and SPAK$^{-/-}$ mice. DCT1 segments, identified by parvalbumin (*green*) and NCC (*red*), are significantly reduced in KO mice. DCT2 segments, indentified by the presence of NCC (*red*) and absence of parvalbumin (*green*) are similar in WT and KO mice (*bar* = 100 μm). As quantified by morphometric analysis, of the DCT, a significant reduction in DCT1 length (*B*) and area (*C*) is noted in the KO mice compared with WT animals. Quantitative summary represent an $n = 4$, *, $p < 0.05$, KO relative to WT. *D,* semiquantitative RT-PCR revealed that the reduction of DCT1 mass in SPAK$^{-/-}$ is paralleled by a decrease in NCC and parvalbumin transcript abundance, whereas the abundance of calbindin D28 (DCT2 and CNT marker) and NKCC2 (TAL marker) transcripts remained unaffected ($n = 4$, *, $p < 0.05$).

contribution to promoting NKCC2 hyperphosphorylation in the SPAK null mice. Other factors are likely involved.

Role of OSR1 and AMPK in the TAL—Examination of OSR1 casts light on its role in the phosphorylation of NKCC2 in young SPAK$^{-/-}$ mice. We found SPAK gene ablation does not alter OSR1 abundance (Fig. 6, *A* and *B*). In the TAL, OSR1 remains at the apical membrane in the phosphorylated, active state (see below), indicating OSR1 has the capacity to *drive* phosphorylation of NKCC2 in SPAK$^{-/-}$ mice. Quantification of the active, phosphorylated forms of SPAK and OSR1 reveals that OSR1 does not undergo a major compensatory activation in the SPAK$^{-/-}$ mice, however. As shown in Fig. 6*C*, phosphorylated forms of OSR1 and SPAK at the highly conserved activation site (SPAK (Ser-383) and OSR1 (Ser-325)) can be detected in Western blot with the anti-pSPAK/pOSR1 Ser-383/Ser-325 antibody. The major phospho-SPAK forms migrate as a 60- and 56-kDa doublet, whereas phospho-OSR1 migrates as a 56-kDa band. Thus, the lower band in the WT mice is a combination of

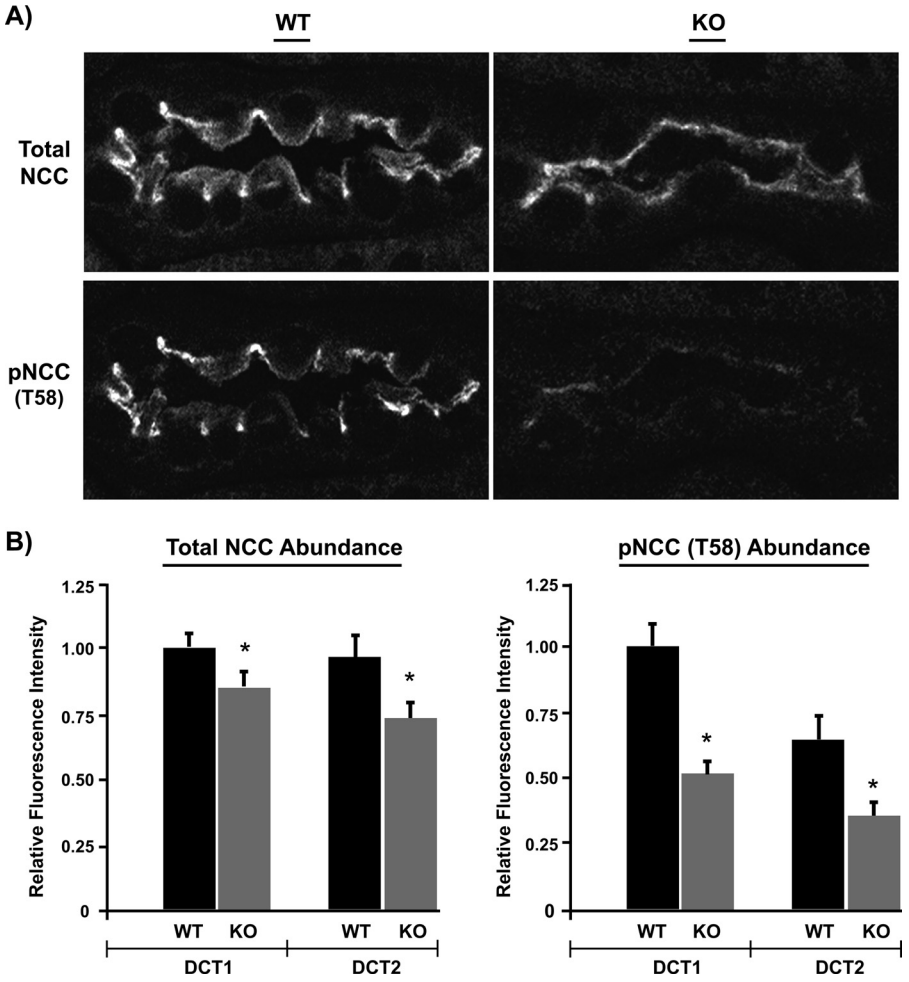

FIGURE 4. **SPAK is required to maintain basal phosphorylation of NCC at the apical surface.** *A,* representative confocal images of NCC (total and phosphorylated (Thr-58)) in remnant DCT of WT and KO ($SPAK^{-/-}$) mice. SPAK gene ablation does not influence apical localization of NCC, but instead reduces the amount of phosphorylated NCC at the apical surface. *B,* quantitative image analysis of NCC abundance (*NCC*) and phosphorylation (*pNCC*) in the DCT1 and DCT2. Relative fluorescence intensity is the apical-delimited intensity relative to the average of the wild-type signal in DCT1. (DCT1 is defined as parvalbumin positive/NCC positive; DCT2 is defined as parvalbumin negative/NCC positive.) Quantitative summary represent an $n = 4$ (70 cells per animal), *, $p < 0.05$, KO relative to the average signal of WT.

phospho-SPAK (pSPAK56) and phospho-OSR1 and it is phospho-OSR1 in the SPAK null mice. Quantification of the bands reveals that the abundance of phospho-OSR1 in SPAK null mice is considerably less (56% less) than the abundance of combined amount of phospho-SPAK and phospho-OSR1 in the WT (Fig. 6*G*). Furthermore, the amount of pOSR1 in SPAK null mice is not increased relative to WT pSPAK56 + pOSR1 (Fig. 6*F*). Thus, OSR1 is available to phosphorylate NKCC2 in SPAK null mice, but its activity is not increased in a way that can easily explain how NKCC2 becomes hyperphosphorylated.

This observation raises the possibility that additional kinases might also be required to enhance NKCC2 phosphorylation in $SPAK^{-/-}$ mice. Because AMP-activated protein kinase (AMPK) has been previously implicated in the regulation of NKCC2 (6), we explored whether this kinase becomes activated in the TAL of SPAK null mice. As shown in Fig. 7 we found for the first time that the abundance of activated-AMPK (pAMPK Thr-172) is increased in SPAK null mice, and the response is restricted to the medulla. As observed by immunofluorescent confocal microscopy, pAMPK becomes co-localized with NKCC2 at the apical membrane of TAL of SPAK null mice. Because AMPK activation (phosphorylation) in heterologous expression systems causes NKCC2 to become phosphorylated at a nearby serine residue (6), our *in vivo* studies suggest that activation of AMPK may be part of the signaling pathway(s) that are responsible for hyperphosphorylation of NKCC2 (see "Discussion"). Obviously, further studies will be required to test the functional relevance of AMPK activation in the activation of NKCC2.

OSR1 Is Dependent on SPAK in the DCT—Another key difference between OSR1/SPAK signaling in the TAL and DCT provides an explanation for the unique requirement of SPAK in the DCT. In contrast to the sustained apical localization and phosphorylation of OSR1 in the TAL, SPAK gene ablation destabilizes apical OSR1 in the DCT. As shown in Fig. 8, OSR1 redistributes to dense punctate structures in both DCT1 and DCT2 of $SPAK^{-/-}$ mice, far removed from NCC at the apical membrane, whereas neighboring TAL maintain strong apical OSR1. Quantification by automated image analysis (by an observer who was blinded as to the groups) revealed that OSR1 puncta are found in nearly all DCT cells of $SPAK^{-/-}$ mice, but only occasionally in WT DCT. Most of these puncta also con-

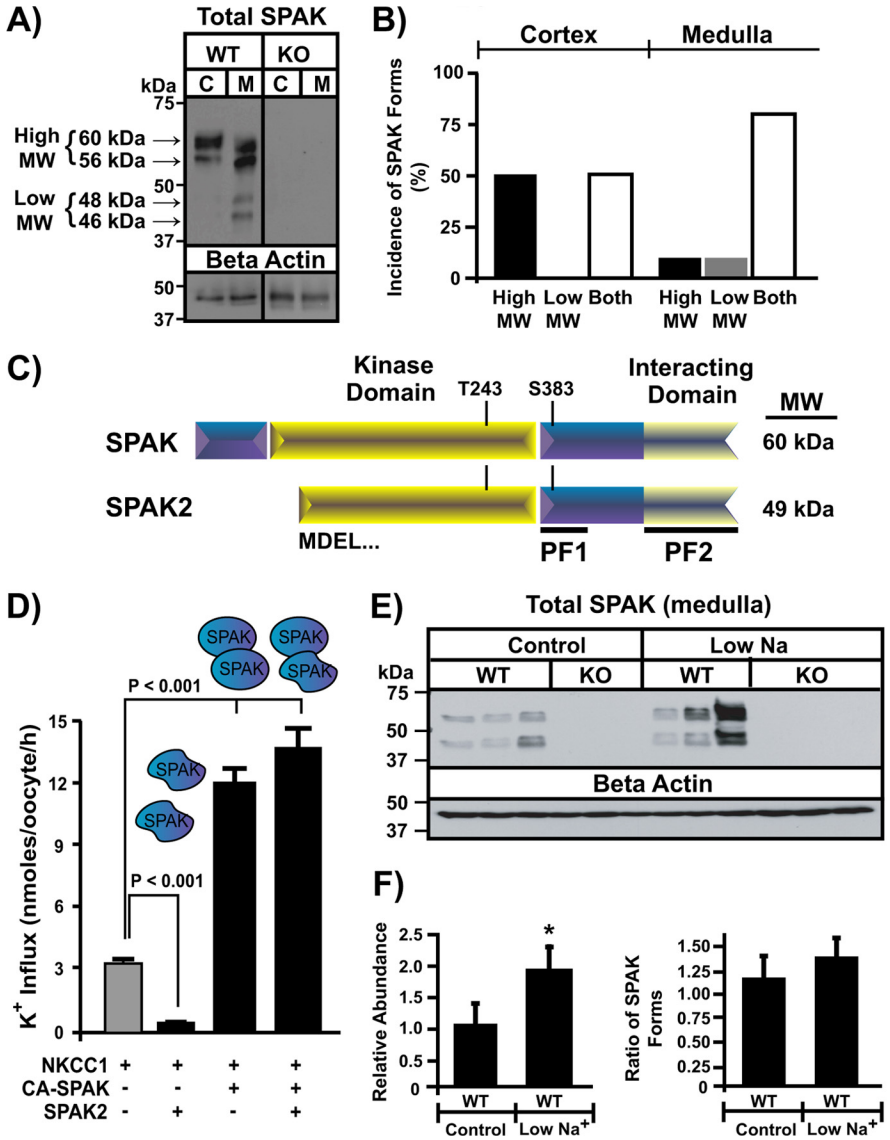

FIGURE 5. **Characterization and function of different SPAK forms in the thick ascending limb and distal convoluted tubule.** *A*, representative Western blot of SPAK in kidney cortex (labeled *C*) or medulla (labeled *M*) of wild-type and SPAK$^{-/-}$ mice. Four forms of SPAK were identified in the WT sample. The two major forms of SPAK (~56 and 60 kDa) migrate near the anticipated molecular mass (*MW*) of full-length SPAK (60 kDa), whereas two smaller SPAK forms (~46 and 48 kDa) in the medulla exhibit a molecular mass close to SPAK2 (48.7 kDa). All SPAK forms are absent in SPAK$^{-/-}$. *B*, the incidence of high and low molecular mass forms in medulla and cortex ($n = 10$ WT). In the cortex, the high molecular mass form is always detected, either alone (50% of samples) or with the low molecular mass form (50%). In medulla, the low molecular mass form is detected more often, either alone (10%) or with the high molecular mass form (80%). *C*, schematic representation of full-length SPAK and SPAK2, an alternatively translated product. The full-length contains a short N terminus (*blue box*) followed by the catalytic domain (*yellow box*). Location of the critical T-loop threonine residue (Thr-243) is indicated. The catalytic domain is followed by a regulatory domain consisting of two protein folds, the PF1 domain proximal to the catalytic domain and which contains the regulatory serine residue (Ser-383) and the PF2 or interacting domain. *D*, NKCC1-mediated K^+ influx in oocytes injected with mouse NKCC1, full-length constitutively active SPAK (CA-SPAK), and SPAK2, as indicated *below the bars*. *Bars* represent mean ± S.E. ($n = 25$ oocytes). *E*, representative Western blot showing the effects of dietary sodium restriction on the abundance of the SPAK forms in the medulla. *F*, quantitative analysis of Western blots reveals that the total abundance of SPAK increases during sodium restriction (*left*), but the ratio of relative abundance (large *versus* small SPAK forms) remains unchanged (*right*). Quantitative summary of total SPAK abundance represent an $n = 6$, *, $p < 0.05$. Relative abundance is the actin-normalized signal relative to the average of the normal sodium. Quantitative summary of the ratio of the abundance of large/small SPAK forms $n = 6$.

tain WNK1 (73 ± 4% of ORS1 containing puncta overlap with WNK1-containing puncta, $n = 8$ animals, 16 tubules examined) as shown in Fig. 8*C*. Moreover, as assessed by the absence of OSR1 phosphorylation at the key activation sites (see Fig. 11*C*, below), OSR1 is inactive in SPAK$^{-/-}$ DCT. Thus, the activity and localization of OSR1 is dependent on SPAK in the DCT. As a consequence, phosphorylation of NCC diminishes in the absence of SPAK. Without active OSR1 or SPAK in SPAK$^{-/-}$ mice, NCC phosphorylation cannot be maintained.

Role of Cab39/MO25α—We also considered the possibility that localization and activation of OSR1 may be controlled in the DCT by SPAK as a result of a mutual dependence on Cab39/MO25α, a putative kinase scaffold that has recently been reported to function as a positive regulator of SPAK and OSR1 *in vitro* (22). Although MO25 was shown to be expressed in the kidney (22), its specific segmental localization in the kidney and possible relationship to sites of SPAK and OSR1 expression has not been described. Fig. 9*B* shows for the first time that MO25α

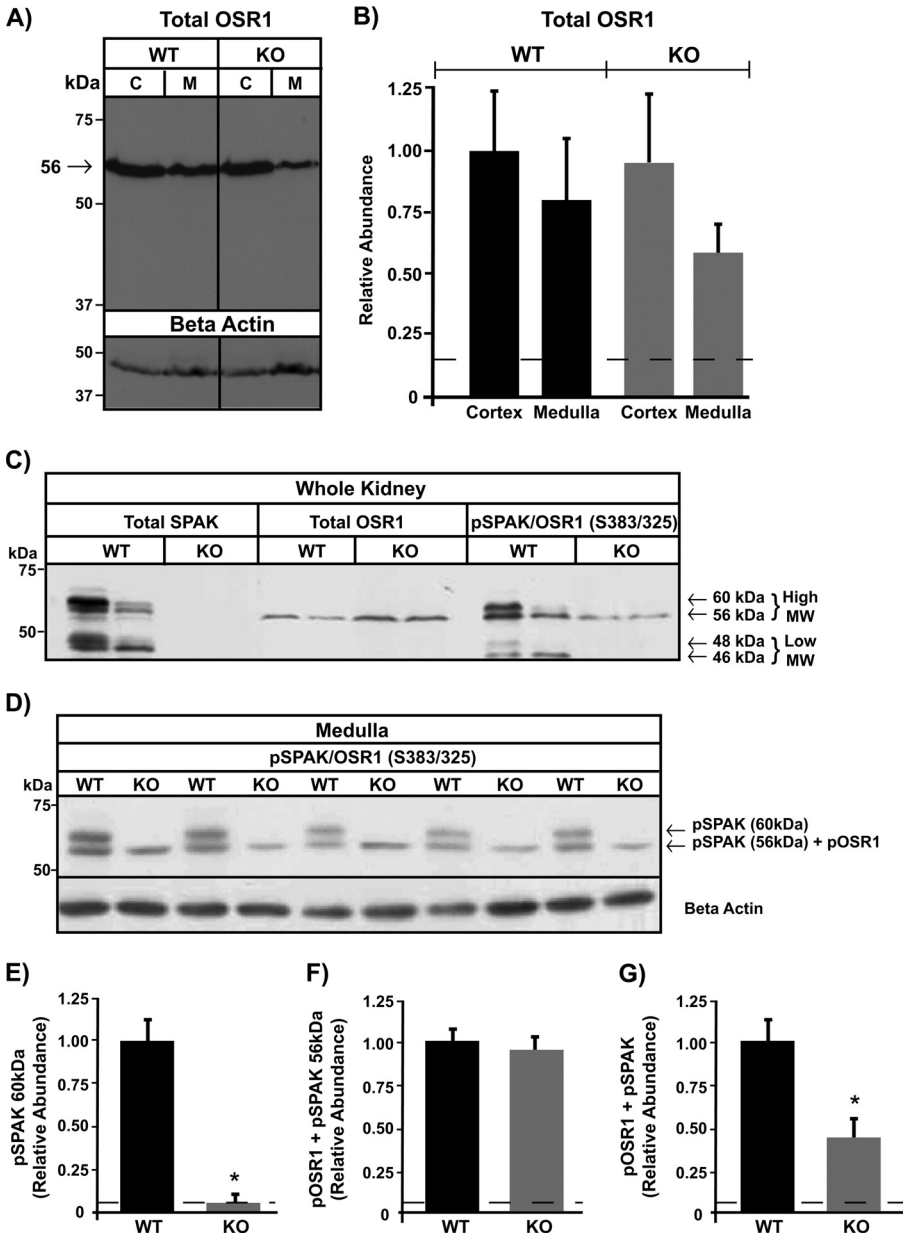

FIGURE 6. **Characterization of OSR1 in the SPAK null (KO).** *A*, representative Western blot and *B*, quantitative summary of OSR1 abundance (total) in kidney cortex (labeled *C*) or medulla (labeled *M*) of wild type and SPAK$^{-/-}$ mice; $n = 3$. Relative abundance is the actin-normalized signal relative to the actin-normalized WT cortex signal. *C*, representative Western blot results showing the migration pattern of total SPAK and OSR1 compared with pSPAK/OSR1 (Ser-383/Ser-325). The major phospho-SPAK forms migrate as a 60- and 56-kDa doublet, whereas phospho-OSR1 migrates as a 56-kDa band. Thus, the lower band in the WT mice is a combination of phospho-SPAK (pSPAK56) and phospho-OSR1 and it is phospho-OSR1 in the SPAK null mice. *D*, representative Western blot results of pSPAK/OSR1 (Ser-383/Ser-325) in kidney medulla of WT and KO mice. Quantitative summary data in *D*, comparing WT *versus* KO of *E;* the abundance of full-length pSPAK (60-kDa band); *F*, the abundance of the 56-kDa pSPAK + OSR1 proteins; and *G*, the abundance of all pSPAK + pOSR1, $n = 5$, *, $p < 0.05$, KO relative to the average normalized signal of WT.

localizes specifically to the DCT and TAL segments. Specific labeling was not detected in other tubular segments such as proximal tubules nor collecting ducts. Remarkably, MO25α colocalized at the apical membrane with NCC and NKCC2 (Fig. 9*C*) in WT mice. As measured by automated image analysis (by an observer who blinded to the groups), apical MO25α labeling was not reduced in DCT of SPAK null mice (Fig. 9*D*). Consistent with this, no difference in the abundance of Cab39/MO25α protein could be detected in the kidney cortex or medulla between WT and SPAK null mice (Fig. 9, *E* and *F*). Taken together, these findings indicate that MO25α has the capacity to function as a regulator of SPAK/OSR1 in the DCT and TAL segments of the kidney. However, because Cab39/MO25α remains at the apical membrane in the SPAK null mice, unlike OSR1, we conclude that Cab39/MO25α is not responsible for controlling the apical localization of OSR1 in the DCT.

SPAK Is Required for Phosphoregulation of NCC in States of Dietary Sodium Restriction

The studies above indicate that localization and function of OSR1 are dependent on SPAK kinase in the DCT, and this relationship is apparently necessary for the basal phosphoryla-

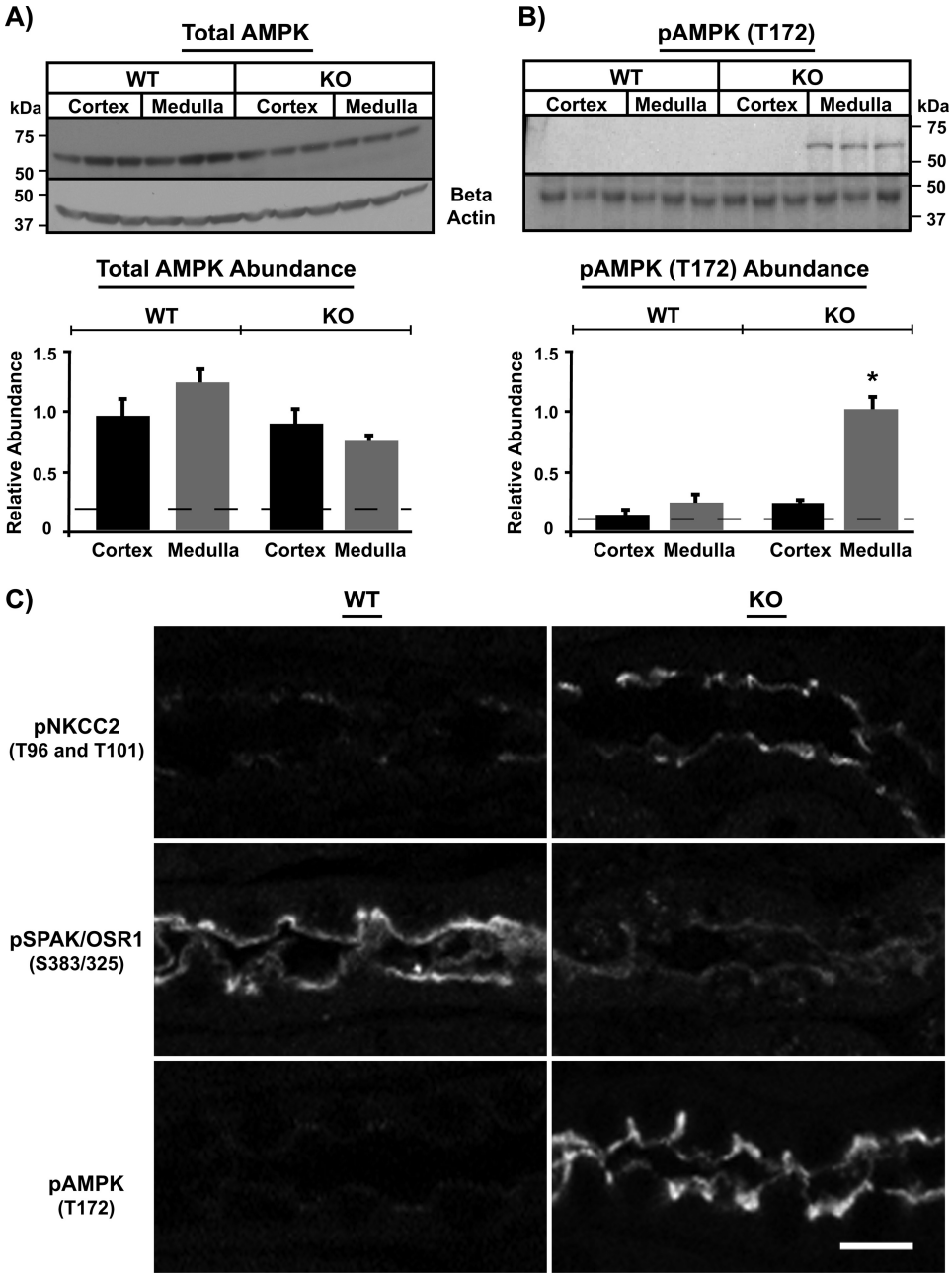

FIGURE 7. **AMPK is selectively activated in TAL of SPAK-null mice.** *A*, Western blot of total AMPK (*left*) and phosphorylated (Thr-172) AMPK (*right*, pAMPK) in kidney cortex and medulla of WT and SPAK KO mice. *B,* quantitative summary, $n = 3$, *, $p < 0.05$. *C,* representative confocal images of phosphorylated NKCC2, SPAK, and AMPK, (phosphorylation sites indicated) in the mTAL or WT and SPAK null mice (KO). Hyperphosphorylation of NKCC2 in the SPAK null occurs concomitantly with an increase in pAMPK at the apical membrane. The decrease in pSPAK/OSR1 is consistent with the Western analysis in Fig. 6.

tion of NCC. SPAK and OSR1 are also suspected to enhance phosphorylation of NCC in response to elevated aldosterone and angiotensin II in states of dietary sodium restriction and intravascular volume depletion, but their role in this important regulatory response has not been directly tested. To explore the requirement of SPAK in physiologic regulation of NCC, we first examined how $SPAK^{-/-}$ mice adapt to dietary sodium restriction (Fig. 10). As evidenced by the elevated rate of urinary sodium excretion (Fig. 10*A*), $SPAK^{-/-}$ mice exhibit a longer period of negative sodium balance after dietary sodium is reduced than the wild-type littermates. Parallel measurements of blood pressure revealed the salt wasting phenotype is manifested in the face of a lower arterial blood pressure (Fig. 10*B*). Such a leftward shift in the relationship between urinary sodium excretion and blood pressure (Fig. 10*C*) is indicative of a primary defect in the sodium reabsorptive capacity of the kidney. It suggests that a greater than normal decrease in arterial blood pressure must occur in the $SPAK^{-/-}$ mice for urinary sodium excretion to be brought into balance with the decrease in dietary sodium load.

As shown in Fig. 11, SPAK gene ablation prevents regulation of NCC by dietary sodium restriction. In wild-type mice, a low sodium diet stimulates a large increase in the abundance and phosphorylation (Thr-58) of NCC at the apical membrane (Fig.

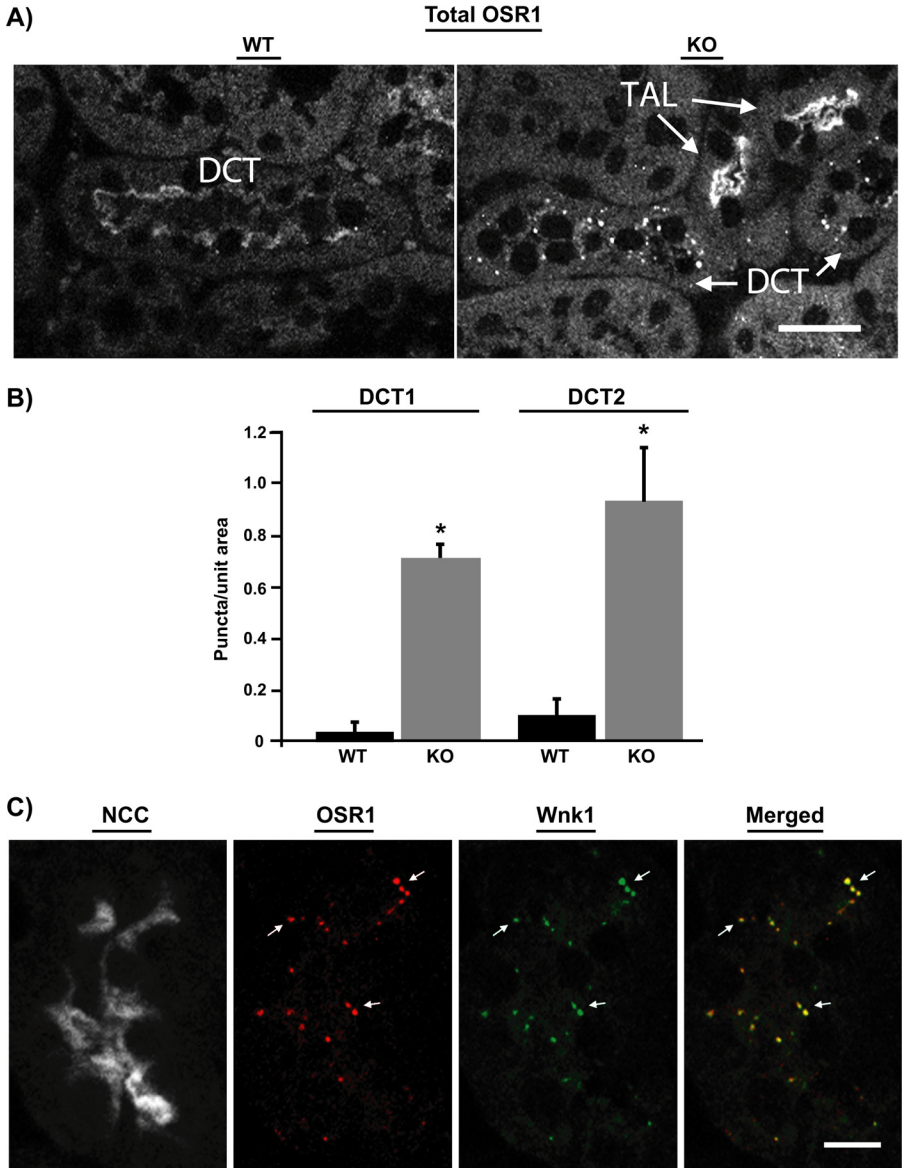

FIGURE 8. **OSR1 localization is dependent on SPAK specifically in the DCT.** *A,* representative confocal images of OSR1 in the kidney of WT and SPAK KO mice. In contrast to the TAL, where OSR1 remains at the apical membrane in the KO, OSR1 becomes displaced from the apical membrane in the DCT, localizing within distinct punctate structures in the cell cytoplasm (*bar* = 20 μm). *B,* quantitative image analysis of puncta number in DCT of wild-type (*WT*) and SPAK KO (*KO*) mice. In contrast to WT cells, nearly all DCT cells in the KO contain OSR1 puncta. DCT1 were identified by the presence of parvalbumin and NCC, whereas DCT2 were defined as parvalbumin negative/NCC positive tubules. $n = 4$ mice, > 20 tubules/mouse, *, $p < 0.05$ compared with WT. *C,* representative confocal image of OSR1 and WNK1 in DCT of SPAK null mouse. WNK1 co-localizes with OSR1 in the puncta (73 $\pm$ 4%, $n = 8$ animals, 3 tubules/mouse; *bar* = 10 μm).

11). As assessed by the parallel increase in phosphorylated SPAK/OSR1 at the apical surface, stimulation of NCC occurs concomitantly with activation of SPAK and OSR1 in WT animals (Fig. 11*C*). In SPAK$^{-/-}$ mice, OSR1 is unable to become similarly activated, remaining in intracellular puncta. Without SPAK or active OSR1 in the DCT of SPAK$^{-/-}$ mice, the normal NCC response to dietary sodium restriction is not observed, although there is a trend for NCC abundance to increase. It is possible that the dystrophic response of the DCT1 in SPAK null mice precludes the detection of a SPAK-independent up-regulation of NCC abundance during dietary sodium restriction. Together these observations identify SPAK and OSR1 as the kinases that phosphorylate and activate NCC in response dietary salt restriction, likely operating as the upstream arbiters of angiotensin II and aldosterone signaling pathways.

DISCUSSION

The present study provides a new understanding of SPAK/OSR1 signaling in the kidney, offering explanations to how SPAK positively regulates salt reabsorption in the DCT while it appears to be inhibitory with respect to NKCC2 in the TAL. Our studies indicate that SPAK co-functions with OSR1 in the DCT, rather than operate as an exclusive activator of NCC as widely believed. We discovered that SPAK is required to control proper apical localization and phosphorylation-dependent activation of OSR1 in the DCT, but not in the TAL. Without SPAK, the signaling system becomes destabilized in the DCT, preventing phosphorylation-dependent activation of NCC-mediated NaCl reabsorption. By contrast, the combined effects of removal of inhibitory putative SPAK2 forms, maintenance of

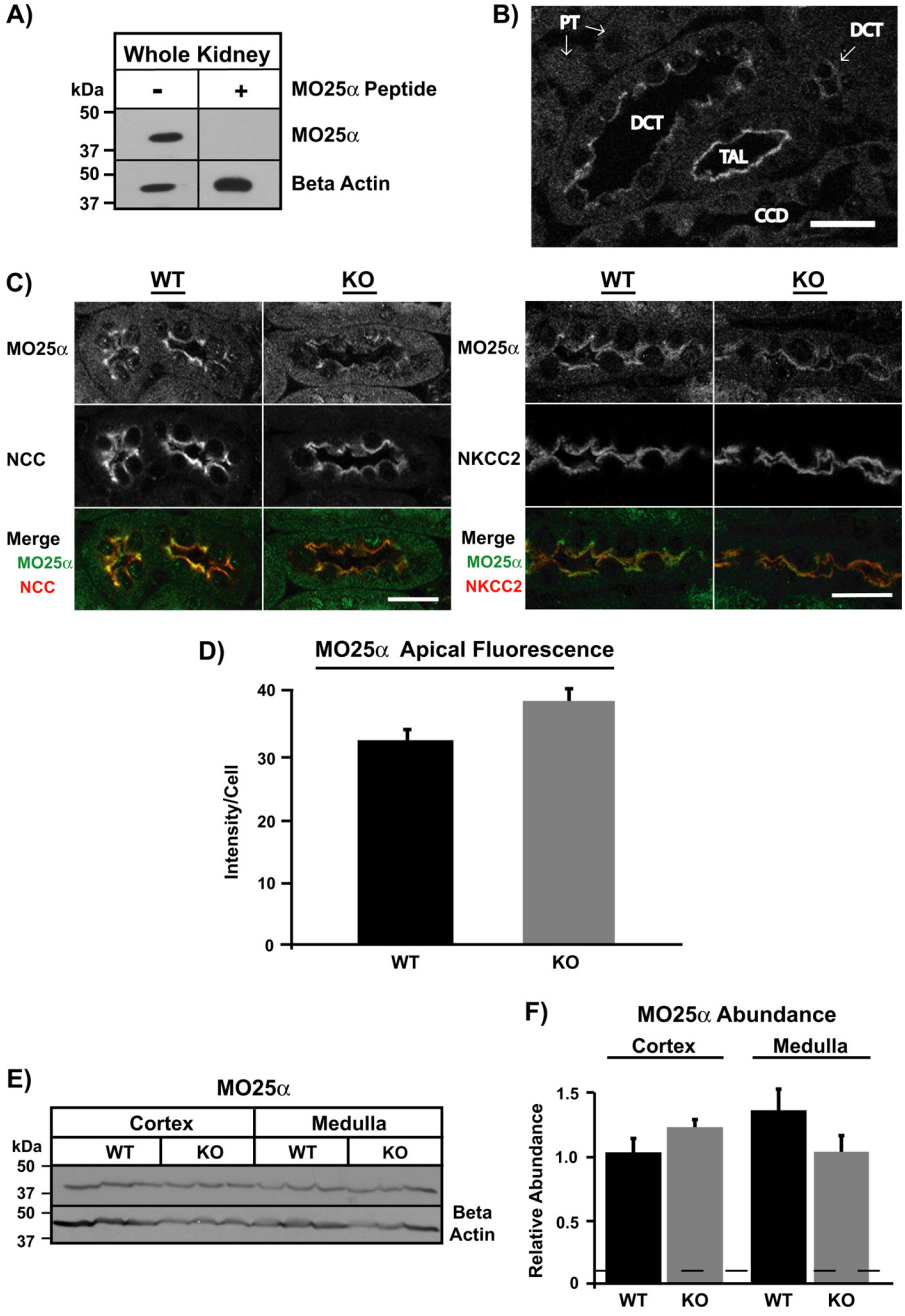

FIGURE 9. **Cab39/MO25α colocalizes with NCC in DCT and NKCC2 in TAL.** *A*, representative Western blot of kidney Cab39/MO25α and actin in the absence (−) and presence (+) of MO25α peptide. *B*, Cab39/MO25α localizes to the apical surface of DCT and TAL and is not detectable in other nephron segments. Segment identity of DCT and TAL was established using antibodies to NCC and NKCC2 (not shown) and structure (proximal tubule (*PT*) and cortical collecting duct (*CCD*)). *Bar* = 20 μm. *C*, representative confocal images of Cab39/MO25α and NCC or NKCC2 in DCT and TAL, respectively, in wild-type (*WT*) and SPAK$^{-/-}$ mice (*KO*) (*bars* = 20 μm). Note co-localization of Cab39/MO25α with the transporters at the apical membrane in WT and KO mice. *D*, quantitative image analysis: summary of MO25α fluorescence intensity at the apical membrane of DCT from WT and KO mice. $n = 4$ animals per group, > 8 tubules/animal. *E*, Western blot of Cab39/MO25α and actin in kidney cortex and medulla from WT and KO mice. *F*, quantitative summary of Cab39/MO25α abundance in kidney cortex and medulla of wild-type and SPAK$^{-/-}$ mice (KO), $n = 3$. Relative abundance is the actin-normalized signal relative to the actin-normalized WT cortex signal.

OSR1 localization, and activation of an AMPK-containing signaling pathway in the TAL may contribute to hyperphosphorylation of NKCC2 in the SPAK KO mouse.

SPAK-OSR1-Cab39/MO25α Signaling Network in the DCT—Our study reveals that the function and localization of OSR1 requires SPAK in the DCT but not the TAL, consistent with the operation of a DCT cell-specific, co-dependent signaling network that regulates NCC phosphorylation. We speculate that this may ensure that both kinases can be simultaneously and optimally phosphorylated for robust activation of NCC. At present, we can only offer conjecture about the basis for kinase co-dependence. A kinase interaction mechanism and the likely role of kinase scaffolds should be considered.

There are indications that OSR1 and SPAK have the capacity to directly interact with each other. The structure of the OSR1 kinase domain, as determined by crystallography, revealed that OSR1 is capable of forming dimers, likely as a part of the kinase activation process (34). Structural elements in OSR1 that are

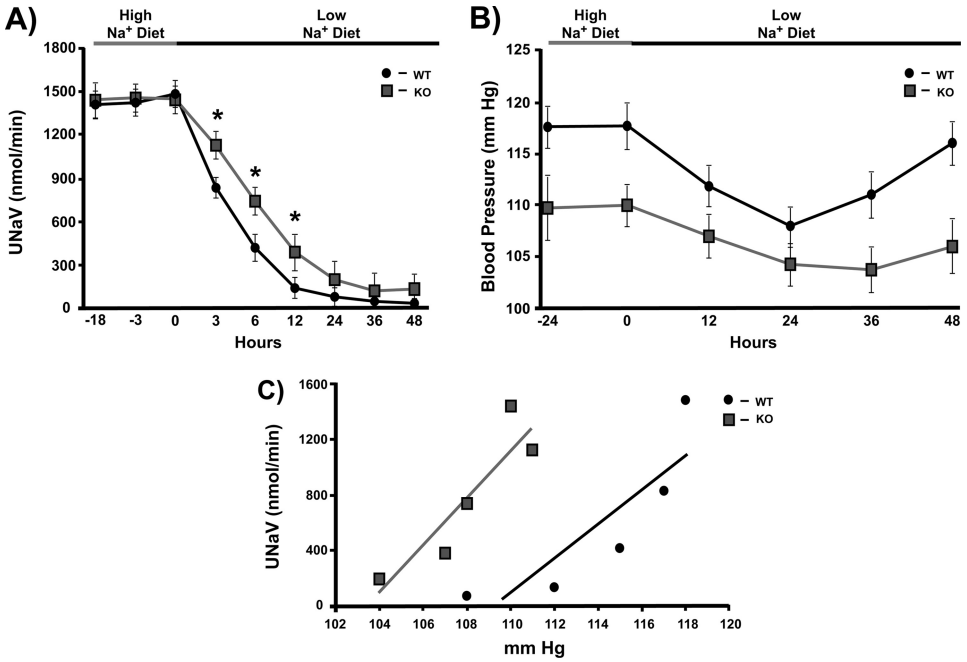

FIGURE 10. **Renal response to dietary sodium restriction is altered in SPAK$^{-/-}$ mice.** *A*, as assessed by rates of urinary sodium excretion ($U_{Na}V$), SPAK$^{-/-}$ mice exhibit a prolonged period of negative sodium balance after dietary sodium is reduced. *B*, parallel measurements of blood pressure revealed the salt wasting phenotype is as occurs in the face of lower arterial blood pressure. *C*, correlation between urinary sodium excretion and blood pressure. SPAK$^{-/-}$ mice have a leftward shift in the pressure-naturiesis relationship, indicative of a primary defect in the sodium reabsorptive capacity of the kidney ($n = 4$; *, $p < 0.05$).

involved in dimerization are also found in SPAK, raising the possibility that SPAK and OSR1 form heterodimers. Thus it will be important for future studies to determine whether this occurs in the kidney and whether heterodimer formation is favored in the DCT, perhaps as a consequence of an optimal abundance of OSR1 and full-length SPAK.

It is also possible that Cab39/MO25α or other scaffolding proteins (35, 36) stabilize SPAK and OSR1 differently in the TAL and DCT. Our new observation that Cab39/MO25α co-localizes with SPAK and OSR1 specifically in the renal DCT and TAL suggests that Cab39/MO25α participates in a functionally important complex with SPAK and OSR1 in both nephron segments as it does with LKB1 and the pseudokinase STRAD in other cells (37). Moreover, because the abundance and localization of Cab39/MO25α are not affected by SPAK gene ablation it is unlikely that Cab39/MO25α is responsible for controlling the apical localization of OSR1 in the DCT. Based on our new localization data and recent reports that Cab39/MO25α facilitates SPAK/OSR1 activation *in vitro* (22), it seems likely that Cab39/MO25α mainly acts as a positive regulator of SPAK and OSR1 in both the TAL and DCT. Obviously, further studies are required to test this idea.

Our studies have a limitation in their ability to fully substantiate the interdependent OSR1/SPAK kinase network hypothesis. Although it is clear that OSR1 is dependent on SPAK in the DCT, it remains to be determined if SPAK is mutually dependent on OSR1. Global kidney-specific OSR1 knock-out mice have been reported recently to exhibit compromised phosphorylation of NKCC2 but not NCC (2), suggesting that OSR1 plays a dominant role in the TAL compared with the DCT. However, because the DCT is well appreciated to undergo an adaptive up-regulation of NaCl reabsorptive transport activity in response to inhibition of sodium reabsorption in the TAL (reviewed in Ref. 32), it is not possible to draw conclusions about the specific role of OSR1 in the DCT from these studies. Future studies with DCT-specific OSR1 knock-out mice will be required to definitively examine whether SPAK is dependent on OSR1 for optimal NCC phosphorylation.

Loss of SPAK Results in DCT1-specific Dystrophic Response—The interdependence of SPAK and OSR1 in DCT may also result from a broader signaling process that controls the differentiation status of DCT1 cells. In fact, we report for the first time that SPAK is required to maintain the structural integrity of DCT1. Our data identify SPAK as an integral part of the signaling pathway that is necessary for DCT1 integrity. The dystrophic response of the DCT1 is similar to what is observed in thiazide diuretic-treated rats (33), NCC KO mice (31), parvalbumin KO mice (39), and mice overexpressing wild-type WNK4 (17). In each instance, NCC-dependent NaCl reabsorption is significantly reduced or eliminated. Furthermore, increased NaCl delivery to the DCT as seen in models of Bartter syndrome (2, 40) results in a *hyper*trophic response in the DCT1. Collectively, these observations are consistent with a positive feedback mechanism that has been proposed to link NaCl entry to the integrity of the early distal tubule (41). Although our studies do not establish that SPAK is a direct arbitor of this response, they demonstrate that SPAK is required to maintain DCT1 mass.

Mechanisms for NKCC2 Hyperphosphorylation in SPAK$^{-/-}$ Mice—Consistent with previous reports (3, 7), we observed that NKCC2 is more phosphorylated in SPAK$^{-/-}$ mice than WT. However, one striking difference between our observations and those reported by McCormick (3) and Yang (7) is that we do not observe an increase in phosphoactivated OSR1 in younger mice, making it unlikely that activation of OSR1, by itself, causes stimulation of NKCC2 phosphorylation. This fortuitous

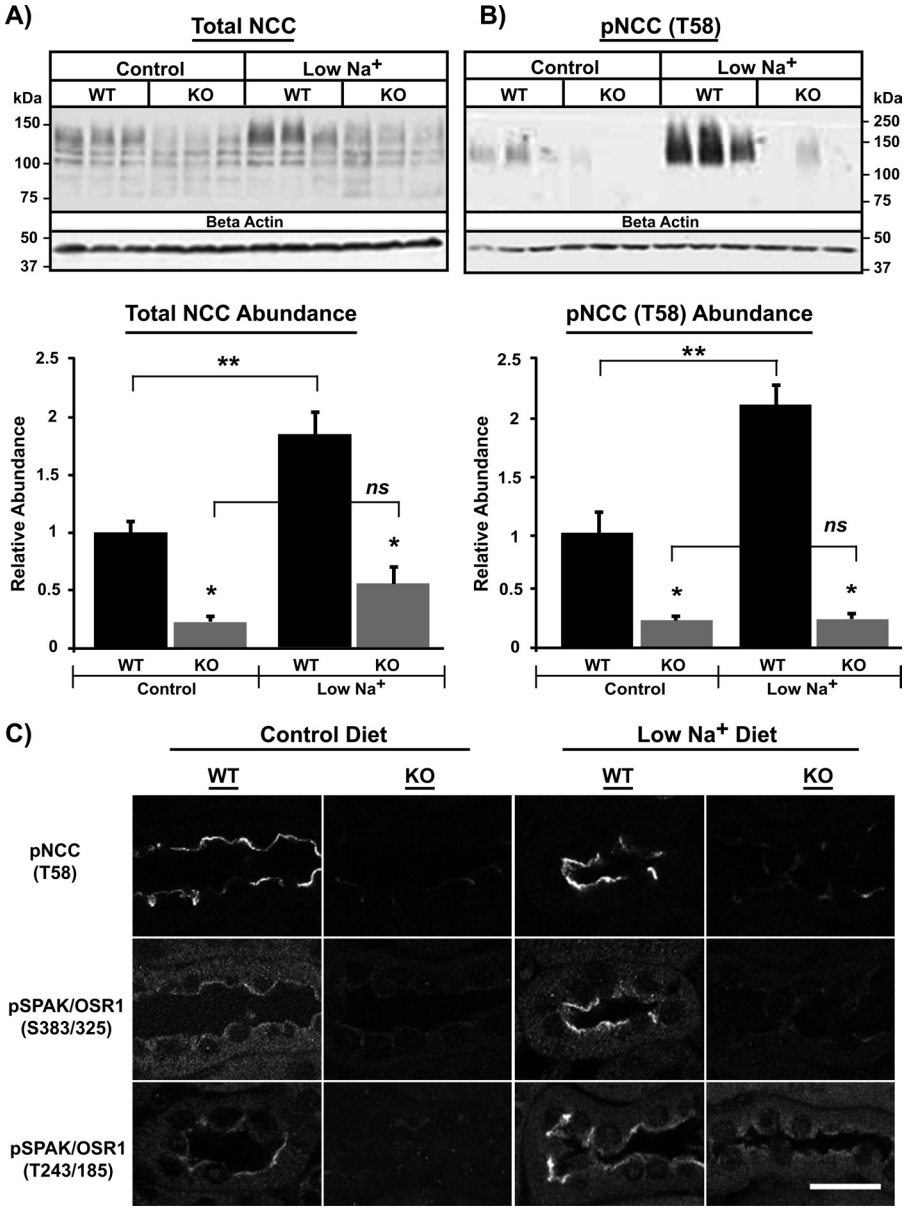

FIGURE 11. **Effect of sodium diet on phosphorylation of NCC and SPAK/OSR1 in DCT.** *A* and *B*, representative Western blots of total (*A*) and phosphorylated (*B*) NCC. Quantitative analysis reveals the abundance of total and phosphorylated NCC increased in WT mice when fed a low sodium diet relative to their control diet counterparts (**, $n = 6$, $p < 0.05$). SPAK$^{-/-}$ mice had significantly less total and phosphorylated NCC than WT littermates (*, $n = 6$, $p < 0.05$) and failed to increase NCC abundance when fed the low sodium diet. *C*, immunolocalization reveals the low sodium diet increased staining of pNCC (Thr-58) and pSPAK/OSR1 (at both the Ser-383/Ser-325 and Thr-243/Thr-185 sites) in WT mice but phosphorylation of OSR1 in SPAK$^{-/-}$ mice is undetectable on control diet and only modestly detectable at the apical surface for mice on the low sodium diet. Note that the prominent punctate OSR1 structures seen in KO animals are not detectably phosphorylated at either site (*bar* = 20 μm).

observation, together with our novel characterization of short SPAK polypeptides in the mouse kidney and of SPAK2 *in vitro*, provides a new understanding of the factors that can provoke NKCC2 phosphorylation in SPAK$^{-/-}$ mice.

Our ideas about the function of the short SPAK forms evolve from the elegant recent studies of McCormick *et al.* (3). Based on the identification of a kidney medulla-specific SPAK transcript (KS-SPAK), which encodes a shorter SPAK protein that lacks the kinase domain and that inhibits phosphorylation of a NKCC2 fragment and NCC by full-length SPAK *in vitro*, McCormick *et al.* (3) proposed that the short SPAK forms act as natural negative kinase inhibitors of NKCC2 phosphorylation in the TAL. According to their idea, NKCC2 becomes hyperphosphorylated in SPAK$^{-/-}$ mice because removal of the shorter "inhibitory" SPAK forms in the TAL causes OSR1 to become more active. Although we do not dispute this might occur, it should be pointed out that the predicted molecular mass of KS-SPAK (34 kDa) is considerably smaller than the short SPAK forms that we detect (~46 and 48 kDa), raising the question whether KS-SPAK is playing a major role in our mice.

Based on size similarity, we propose that a short SPAK form in the mouse kidney corresponds to SPAK2, an isoform generated by alterative initiation of translation, 115 base pairs 3′ from the full-length SPAK initiation site (27), or a comparable proteolytic fragment. Like KS-SPAK, we found that SPAK2 exerts inhibitory activity on NKCC1 *in vitro*. NKCC1 and NKCC2

have nearly identical phosphorylation and binding sites for SPAK/OSR1, so results with NKCC1 can be extrapolated to NKCC2. Because SPAK2 lacks the first three β sheets of the N-lobe in the kinase domain, including a key lysine residue that forms an ion pair with a key catalytic glutamic acid residue in helix αC in active kinases, but retains the C-terminal substrate binding domain, it is highly likely that SPAK2 is a catalytically impaired isoform that is capable of interacting with the co-transporters. As a consequence, SPAK2 likely competes with the native kinases (OSR1 in *Xenopus* oocytes, full-length SPAK and OSR1 in TAL) for the RF*X*(V/I) motifs on the cotransporters, and blocks activation by occluding the phosphorylation site and/or interaction site of the transporter for the full-length kinase.

The SPAK2 competition mechanism is consistent with our observation that hyperphosphorylation of NKCC2 occurs without a major increase in phosphoactive OSR1 in SPAK$^{-/-}$ mice, but does not offer a complete explanation for the increased NKCC2 phosphorylation. Unlike KS-SPAK, SPAK2 does not exhibit robust inhibitory effects on the function of the constitutively active kinase, especially when the full-length SPAK is equally as abundant. This is significant because the abundance of the putative SPAK2 form was found equal to the full-length SPAK in the kidney medulla. Taken together, these observations imply that the inhibitory output of SPAK2 is unlikely to exceed the stimulatory output of full-length SPAK in the wild-type TAL. As such, ablation of SPAK gene expression may not necessarily lead to a large increase in NKCC2 phosphorylation.

Other signaling pathways are likely to be at play. Evidence for this idea is provided by our new observation that another kinase, AMPK, is specifically activated at the TAL apical membrane in SPAK null mice, concomitantly with NKCC2 phosphorylation. AMP-activated kinase has been shown to phosphorylate the co-transporter *in vitro* (6, 38), raising the possibility that this kinase is directly responsible. It should be pointed out, however, when activated in HEK293 (6), AMPK primarily phosphorylates a different key NKCC2 activation site, Ser-126 (mouse sequence), than phosphorylated by OSR1/SPAK (*i.e.* Thr-96 and Thr-101). Additionally, although the activation of AMPK and its localization in TAL support this model, it has yet to be shown that AMPK is necessary/sufficient for NKCC2 hyperphosphorylation. We speculate that activation of AMPK in the SPAK null is a part of a broader signaling pathway that is stimulated to enhance NKCC2 phosphorylation at all the key activation residues and, thereby increase TAL salt-reabsorption to restore the intravascular volume. Obviously, further studies are required to more completely identify the nature of this pathway.

Summary—Thiazide-sensitive sodium reabsorption is especially dependent on SPAK because the full-length form of the kinase acts as an integral part of a DCT-specific signaling system with OSR1 and Cab39/MO25α to positively regulate the activity of NCC by phosphorylation. Removal of the inhibitory SPAK2 in the TAL, together with maintained OSR1 activity, and activation of a compensatory signaling pathway, which may involve AMPK, allows NKCC2 to become hyperphosphorylated in the SPAK null mouse.

REFERENCES

1. Chiga, M., Rai, T., Yang, S. S., Ohta, A., Takizawa, T., Sasaki, S., and Uchida, S. (2008) Dietary salt regulates the phosphorylation of OSR1/SPAK kinases and the sodium chloride cotransporter through aldosterone. *Kidney Int.* **74,** 1403–1409
2. Lin, S. H., Yu, I. S., Jiang, S. T., Lin, S. W., Chu, P., Chen, A., Sytwu, H. K., Sohara, E., Uchida, S., Sasaki, S., and Yang, S. S. (2011) Impaired phosphorylation of Na^+-K^+-2Cl^- cotransporter by oxidative stress-responsive kinase-1 deficiency manifests hypotension and Bartter-like syndrome. *Proc. Natl. Acad. Sci. U.S.A.* **108,** 17538–17543
3. McCormick, J. A., Mutig, K., Nelson, J. H., Saritas, T., Hoorn, E. J., Yang, C. L., Rogers, S., Curry, J., Delpire, E., Bachmann, S., and Ellison, D. H. (2011) A SPAK isoform switch modulates renal salt transport and blood pressure. *Cell Metab.* **14,** 352–364
4. Rafiqi, F. H., Zuber, A. M., Glover, M., Richardson, C., Fleming, S., Jovanovipć, S., Jovanović, A., O'Shaughnessy, K. M., and Alessi, D. R. (2010) Role of the WNK-activated SPAK kinase in regulating blood pressure. *EMBO Mol. Med.* **2,** 63–75
5. Richardson, C., Rafiqi, F. H., Karlsson, H. K., Moleleki, N., Vandewalle, A., Campbell, D. G., Morrice, N. A., and Alessi, D. R. (2008) Activation of the thiazide-sensitive Na^+-Cl^- cotransporter by the WNK-regulated kinases SPAK and OSR1. *J. Cell Sci.* **121,** 675–684
6. Richardson, C., Sakamoto, K., de los Heros, P., Deak, M., Campbell, D. G., Prescott, A. R., and Alessi, D. R. (2011) Regulation of the NKCC2 ion cotransporter by SPAK-OSR1-dependent and -independent pathways. *J. Cell Sci.* **124,** 789–800
7. Yang, S. S., Lo, Y. F., Wu, C. C., Lin, S. W., Yeh, C. J., Chu, P., Sytwu, H. K., Uchida, S., Sasaki, S., and Lin, S. H. (2010) SPAK-knockout mice manifest Gitelman syndrome and impaired vasoconstriction. *J. Am. Soc. Nephrol.* **21,** 1868–1877
8. Delpire, E. (2009) The mammalian family of sterile 20p-like protein kinases. *Pflugers Arch.* **458,** 953–967
9. Delpire, E., and Gagnon, K. B. (2008) SPAK and OSR1. STE20 kinases involved in the regulation of ion homoeostasis and volume control in mammalian cells. *Biochem. J.* **409,** 321–331
10. Pacheco-Alvarez, D., Cristóbal, P. S., Meade, P., Moreno, E., Vazquez, N., Muñoz, E., Díaz, A., Juárez, M. E., Giménez, I., and Gamba, G. (2006) The Na^+:Cl^- cotransporter is activated and phosphorylated at the amino-terminal domain upon intracellular chloride depletion. *J. Biol. Chem.* **281,** 28755–28763
11. Gagnon, K. B., England, R., and Delpire, E. (2006) Characterization of SPAK and OSR1, regulatory kinases of the Na-K-2Cl cotransporter. *Mol. Cell. Biol.* **26,** 689–698
12. Piechotta, K., Lu, J., and Delpire, E. (2002) Cation chloride cotransporters interact with the stress-related kinases Ste20-related proline-alanine-rich kinase (SPAK) and oxidative stress response 1 (OSR1). *J. Biol. Chem.* **277,** 50812–50819
13. Simon, D. B., and Lifton, R. P. (1996) The molecular basis of inherited hypokalemic alkalosis. Bartter and Gitelman syndromes. *Am. J. Physiol.* **271,** F961-F966
14. San-Cristobal, P., Pacheco-Alvarez, D., Richardson, C., Ring, A. M., Vazquez, N., Rafiqi, F. H., Chari, D., Kahle, K. T., Leng, Q., Bobadilla, N. A., Hebert, S. C., Alessi, D. R., Lifton, R. P., and Gamba, G. (2009) Angiotensin II signaling increases activity of the renal Na-Cl cotransporter through a WNK4-SPAK-dependent pathway. *Proc. Natl. Acad. Sci. U.S.A.* **106,** 4384–4389
15. Vallon, V., Schroth, J., Lang, F., Kuhl, D., and Uchida, S. (2009) Expression and phosphorylation of the Na^+-Cl^- cotransporter NCC *in vivo* is regulated by dietary salt, potassium, and SGK1. *Am. J. Physiol. Renal Physiol.* **297,** F704–712
16. Schambelan, M., Sebastian, A., and Rector, F. C., Jr. (1981) Mineralocorticoid-resistant renal hyperkalemia without salt wasting (type II pseudohypoaldosteronism). Role of increased renal chloride reabsorption. *Kidney Int.* **19,** 716–727
17. Lalioti, M. D., Zhang, J., Volkman, H. M., Kahle, K. T., Hoffmann, K. E., Toka, H. R., Nelson-Williams, C., Ellison, D. H., Flavell, R., Booth, C. J., Lu, Y., Geller, D. S., and Lifton, R. P. (2006) Wnk4 controls blood pressure and

potassium homeostasis via regulation of mass and activity of the distal convoluted tubule. *Nat. Genet.* **38,** 1124–1132
18. Yang, C. L., Zhu, X., Wang, Z., Subramanya, A. R., and Ellison, D. H. (2005) Mechanisms of WNK1 and WNK4 interaction in the regulation of thiazide-sensitive NaCl cotransport. *J. Clin. Invest.* **115,** 1379–1387
19. Wilson, F. H., Disse-Nicodème, S., Choate, K. A., Ishikawa, K., Nelson-Williams, C., Desitter, I., Gunel, M., Milford, D. V., Lipkin, G. W., Achard, J. M., Feely, M. P., Dussol, B., Berland, Y., Unwin, R. J., Mayan, H., Simon, D. B., Farfel, Z., Jeunemaitre, X., and Lifton, R. P. (2001) Human hypertension caused by mutations in WNK kinases. *Science* **293,** 1107–1112
20. Gordon, R. D. (1986) Syndrome of hypertension and hyperkalemia with normal glomerular filtration rate. *Hypertension* **8,** 93–102
21. Castañeda-Bueno, M., Cervantes-Pérez, L. G., Vázquez, N., Uribe, N., Kantesaria, S., Morla, L., Bobadilla, N. A., Doucet, A., Alessi, D. R., and Gamba, G. (2012) Activation of the renal Na^+:Cl^- cotransporter by angiotensin II is a WNK4-dependent process. *Proc. Natl. Acad. Sci. U.S.A.* **109,** 7929–7934
22. Filippi, B. M., de los Heros, P., Mehellou, Y., Navratilova, I., Gourlay, R., Deak, M., Plater, L., Toth, R., Zeqiraj, E., and Alessi, D. R. (2011) MO25 is a master regulator of SPAK/OSR1 and MST3/MST4/YSK1 protein kinases. *EMBO J.* **30,** 1730–1741
23. Gagnon, K. B., Rios, K., and Delpire, E. (2011) Functional insights into the activation mechanism of Ste20-related kinases. *Cell Physiol. Biochem.* **28,** 1219–1230
24. Geng, Y., Hoke, A., and Delpire, E. (2009) The Ste20 kinases Ste20-related proline-alanine-rich kinase and oxidative-stress response 1 regulate NKCC1 function in sensory neurons. *J. Biol. Chem.* **284,** 14020–14028
25. Kim, G. H., Ecelbarger, C. A., Mitchell, C., Packer, R. K., Wade, J. B., and Knepper, M. A. (1999) Vasopressin increases Na-K-2Cl cotransporter expression in thick ascending limb of Henle loop. *Am. J. Physiol.* **276,** F96-F103
26. Flemmer, A. W., Gimenez, I., Dowd, B. F., Darman, R. B., and Forbush, B. (2002) Activation of the Na-K-Cl cotransporter NKCC1 detected with a phosphospecific antibody. *J. Biol. Chem.* **277,** 37551–37558
27. Piechotta, K., Garbarini, N., England, R., and Delpire, E. (2003) Characterization of the interaction of the stress kinase SPAK with the Na^+-K^+-$2Cl^-$ cotransporter in the nervous system. Evidence for a scaffolding role of the kinase. *J. Biol. Chem.* **278,** 52848–52856
28. Coleman, R. A., Wu, D. C., Liu, J., and Wade, J. B. (2000) Expression of aquaporins in the renal connecting tubule. *Am. J. Physiol. Renal Physiol.* **279,** F874–F883
29. Merz, W. A. (1968) Die Strecken messung an gerichteten Struktwuren in Mikroskop und ihre Anwedung zur Bestimmung von Oberflachen-Volumen-Relationen im Knochengewebe. *Mikroskopie* **22,** 132–142
30. Delpire, E., and Gagnon, K. B. (2011) Kinetics of hyperosmotically stimulated Na-K-2Cl cotransporter in *Xenopus laevis* oocytes. *Am. J. Physiol. Cell Physiol.* **301,** C1074–1085
31. Loffing, J., Vallon, V., Loffing-Cueni, D., Aregger, F., Richter, K., Pietri, L., Bloch-Faure, M., Hoenderop, J. G., Shull, G. E., Meneton, P., and Kaissling, B. (2004) Altered renal distal tubule structure and renal Na^+ and Ca^{2+} handling in a mouse model for Gitelman's syndrome. *J. Am. Soc. Nephrol.* **15,** 2276–2288
32. Reilly, R. F., and Ellison, D. H. (2000) Mammalian distal tubule. Physiology, pathophysiology, and molecular anatomy. *Physiol. Rev.* **80,** 277–313
33. Loffing, J., Loffing-Cueni, D., Hegyi, I., Kaplan, M. R., Hebert, S. C., Le Hir, M., and Kaissling, B. (1996) Thiazide treatment of rats provokes apoptosis in distal tubule cells. *Kidney Int.* **50,** 1180–1190
34. Lee, S. J., Cobb, M. H., and Goldsmith, E. J. (2009) Crystal structure of domain-swapped STE20 OSR1 kinase domain. *Protein Sci.* **18,** 304–313
35. Reiche, J., Theilig, F., Rafiqi, F. H., Carlo, A. S., Militz, D., Mutig, K., Todiras, M., Christensen, E. I., Ellison, D. H., Bader, M., Nykjaer, A., Bachmann, S., Alessi, D., and Willnow, T. E. (2010) SORLA/SORL1 functionally interacts with SPAK to control renal activation of Na^+-K^+-Cl^- cotransporter 2. *Mol. Cell Biol.* **30,** 3027–3037
36. Carmosino, M., Rizzo, F., Procino, G., Basco, D., Valenti, G., Forbush, B., Schaeren-Wiemers, N., Caplan, M. J., and Svelto, M. (2010) MAL/VIP17, a new player in the regulation of NKCC2 in the kidney. *Mol. Biol. Cell* **21,** 3985–3997
37. Zeqiraj, E., Filippi, B. M., Deak, M., Alessi, D. R., and van Aalten, D. M. (2009) Structure of the LKB1-STRAD-MO25 complex reveals an allosteric mechanism of kinase activation. *Science* **326,** 1707–1711
38. Fraser, S. A., Gimenez, I., Cook, N., Jennings, I., Katerelos, M., Katsis, F., Levidiotis, V., Kemp, B. E., and Power, D. A. (2007) Regulation of the renal-specific Na^+-K^+-$2Cl^-$ co-transporter NKCC2 by AMP-activated protein kinase (AMPK). *Biochem. J.* **405,** 85–93
39. Belge, H., Gailly, P., Schwaller, B., Loffing, J., Debaix, H., Riveira-Munoz, E., Beauwens, R., Devogelaer, J. P., Hoenderop, J. G., Bindels, R. J., and Devuyst, O. (2007) Renal expression of parvalbumin is critical for NaCl handling and response to diuretics. *Proc. Natl. Acad. Sci. U.S.A.* **104,** 14849–14854
40. Wagner, C. A., Loffing-Cueni, D., Yan, Q., Schulz, N., Fakitsas, P., Carrel, M., Wang, T., Verrey, F., Geibel, J. P., Giebisch, G., Hebert, S. C., and Loffing, J. (2008) Mouse model of type II Bartter syndrome. II. Altered expression of renal sodium and water-transporting proteins. *Am. J. Physiol. Renal Physiol.* **294,** F1373–1380
41. Stanton, B. A., and Kaissling, B. (1989) Regulation of renal ion transport and cell growth by sodium. *Am. J. Physiol.* **257,** F1–10